

1 Graphene Multiplexed Sensor for 2 Point-of-Need Viral Wastewater-Based 3 Epidemiology

4 Michael Geiwitz¹, Owen Rivers Page², Tio Marelllo¹, Narendra Kumar³, Stephen Hummel⁴, Vsevolod
5 Belosevich¹, Qiong Ma¹, Tim van Opijnen², Bruce Batten³, Michelle M. Meyer², Kenneth S. Burch^{1*}

6 ¹ Department of Physics, Boston College, Chestnut Hill, MA 02467, USA

7 ² Department of Biology, Boston College, Chestnut Hill, MA 02467, USA

8 ³ GRIP Molecular Technologies, Inc., 1000 Westgate Drive, Saint Paul, MN 55114, USA

9 ⁴ Department of Chemistry and Life Science, United States Military Academy, West Point, NY 10996, USA

10 Abstract

11 Wastewater-based epidemiology (WBE) can help mitigate the spread of respiratory infections
12 through the early detection of viruses, pathogens, and other biomarkers in human waste. The need for
13 sample collection, shipping, and testing facilities drives up the cost of WBE and hinders its use for rapid
14 detection and isolation in environments with small populations and in low-resource settings. Given the
15 ubiquitousness and regular outbreaks of respiratory syncytial virus, SARS-CoV-2 and various influenza
16 strains, there is a rising need for a low-cost and easy-to-use biosensing platform to detect these viruses
17 locally before outbreaks can occur and monitor their progression. To this end, we have developed an
18 easy-to-use, cost-effective, multiplexed platform able to detect viral loads in wastewater with several

*Corresponding author at: Department of Physics, Boston College, Chestnut Hill, MA 02467, USA

Email address: ks.burch@bc.edu (K.S. Burch)

NOTE: This preprint reports new research that has not been certified by peer review and should not be used to guide clinical practice.

19 orders of magnitude lower limit of detection than mass spectrometry. This is enabled by wafer scale
20 production and aptamers pre-attached with linker molecules, producing forty-four chips at once. Each
21 chip can simultaneously detect four target analytes using twenty transistors segregated into four sets of
22 five for each analyte to allow for immediate statistical analysis. We show our platform's ability to rapidly
23 detect three virus proteins (SARS-CoV-2, RSV, and Influenza A) and a population normalization molecule
24 (caffeine) in wastewater. Going forward, turning these devices into hand-held systems would enable
25 waste-water epidemiology in low-resource settings and be instrumental for rapid, local outbreak
26 prevention.

27 **Keywords**

28 SARS-CoV-2; Influenza; Respiratory syncytial virus; Graphene field effect transistor (GFET); Caffeine;
29 Aptamer

30 **1. Introduction**

31 According to the World Health Organization, lower respiratory infections are the fourth leading
32 cause of death worldwide and second in low-income countries (World Health Organization 2014). The
33 top three causes for these infections are SARS-CoV-2, Influenza, and Respiratory Syncytial Virus (RSV)
34 (Madhi et al. 2020; Rouzé et al. 2021; Lafond et al. 2021). There is a growing emphasis on wastewater-
35 based epidemiology (WBE) to track outbreaks. However, WBE is predominantly performed in high-
36 income countries and densely populated areas (Ahmed et al. 2020; Hart and Halden 2020; Medema et
37 al. 2020). Furthermore, if detection can occur on site, WBE would be instrumental to mitigating and
38 tracking outbreaks from these viruses via early detection of viruses and other pathogens shed by
39 asymptomatic carriers without requiring invasive and frequent individual tests (Champredon and
40 Vanrolleghem 2023). For example, SARS-Cov-2 RNA can be detectable in wastewater 5 – 8 days before

41 symptom onset and 2 – 4 days before positive clinical PCR tests (Peccia et al. 2020; Nemudryi et al.
42 2020).

43 Indeed, several college campuses exploited existing testing infrastructure to employ highly
44 localized wastewater testing to prevent outbreaks during the Covid-19 pandemic. An instructive
45 example is the University of California San Diego (UCSD), where sampling from 239 buildings across their
46 campus allowed early hot spot detection and individual testing on a per-building basis (Karthikeyan et al.
47 2021, 2022). UCSD diagnosed nearly 85% of all SARS-CoV-2 infections on campus early and implemented
48 preventative measures to mitigate the spread of the virus (Karthikeyan et al. 2021). This localized
49 approach to WBE could also benefit low- and middle-income countries, where sewage is typically
50 collected in individual or partially shared reservoirs (Street et al. 2020) that are not connected to
51 community sewage systems (Adelodun et al. 2020). This is particularly relevant to RSV, a leading cause
52 of respiratory-related deaths in those 0 – 5 years old (CDC 2023), where data from low- and middle-
53 income countries is lacking or missing altogether due to inadequate systems and infrastructure needed
54 to track disease transmission (Pawar 2023). Even in high-resource settings, the typical collection at a
55 central waste-water facility limits sensitivity of pathogen detection in wastewater due to short half-lives
56 of analytes of interest (Hart and Halden 2020) and natural dilution (Lowry, Wolfe, and Boehm 2023) of
57 target biomarkers.

58 Several factors have hindered the widespread adoption of WBE and led to the general reliance
59 on sample collection at centralized treatment facilities. Specifically, WBE testing is performed almost
60 entirely utilizing advanced techniques in analytical chemistry and molecular biology, including liquid
61 chromatography-mass spectrometry (LC-MS), high-pressure liquid chromatography-mass spectrometry
62 (HPLC-MS), digital polymerase chain reaction, or real-time quantitative polymerase chain reaction (RT-
63 qPCR) that requires dedicated lab space, personnel, equipment, and chemicals (Lorenzo and Picó 2019).
64 Limited testing facilities and the need for sample collection and transport can also delay results and

65 response times, limiting WBE for effective outbreak prevention (Leung 2021). Indeed, the WBE company
66 BioBot in Cambridge, MA, says their average testing time is 11 – 15 days due to the need to test from
67 multiple districts in weekly batches, creating a sample testing backlog (Biobot 2023b). Due to dilution of
68 fecal waste in municipal wastewater, LC-MS and RT-qPCR rely on filtering and concentrating the
69 collected sample (Adams 2020; Li, Wnkui; Zhang, Ji; Tse 2013), with HPLC-MS also subjecting it to several
70 high-pressure steps to separate constituent elements (Else et al. 2010; Metabolite et al. 2023). Thus, a
71 low-cost, easy-to-use, multiplexed device is urgently needed to enable point-of-need WBE.

72 Particularly challenging is the need of a sensing platform to withstand the harsh wastewater
73 medium while accurately and reliably distinguishing between the various components. Wastewater can
74 contain viruses shed in human waste and other particles ranging from naturally occurring biomass,
75 bacteria strains, and drug metabolites to pharmaceuticals (Massano et al. 2023). Similarly challenging is
76 the need to multiplex assays or testing strategies to monitor multiple targets to reduce cost, time, and
77 effort while addressing seasonal and population variations via normalization. For point-of-need WBE
78 sensing, population normalization is crucial due to increased variability in dilution factors, such as per
79 capita water use, stormwater inputs, etc., and viral shedding rates (Sweetapple et al. 2023; Rainey et al.
80 2023; C. Li et al. 2022a). This variability exacerbates the already challenging task of calculating the
81 number of people infected based solely on the virus concentration in the wastewater sample. For
82 example, depending on the level of infection, a person suffering from SARS-CoV-2 can excrete anywhere
83 from 600,000 (N. Zhang et al. 2020) to 30,000,000 virions/L (Wölfel et al. 2020) of fecal matter.

84 To enable WBE at the local level, especially in low-resource and rural communities, it is helpful
85 to look towards efforts in personalized health care. Substantial efforts have been made regarding
86 sensing respiratory infections using lateral flow immunoassay (LFIA), low-cost PCR, and electronic
87 sensors. Electronic sensors are potentially the most promising as they can simultaneously offer
88 multiplexed, low-cost, high sensitivity detection with minimal human effort. Here, there is growing

89 interest in graphene field effect transistors (GFET), which have shown the capability to detect everything
90 from lead ions (Velusamy et al. 2022; Dong et al. 2023) to bacteria and oral disease biomarkers (Ping et
91 al. 2016b; Gao et al. 2016; Kumar, Gray, et al. 2020), though few have shown multiplexing capabilities
92 (Lu et al. 2022; Kumar et al. 2022; Kumar, Gray, et al. 2020). Nonetheless, only two groups, including
93 ours, have demonstrated GFET's use for detection of analytes in wastewater. For instance, a GFET
94 recently detected cadmium ions in wastewater with a limit of detection (LOD) of 0.125 pM (H. Wang et
95 al. 2023). Still, virus protein detection in wastewater with GFETs, let alone by a scalable fabrication
96 method, has not been shown.

97 This work focused on developing wafer-scale fabrication of GFET devices for rapid, easy-to-use,
98 low-cost, multiplexed, and population-normalized detection of respiratory viruses in wastewater at low
99 levels of detection (LOD). To do so, we implemented a new probe strategy where aptamers, single-
100 stranded oligonucleotides, are pre-attached to the linker molecule, removing the need for harsh
101 solvents. This enhanced the device's reproducibility, lowering filtration levels and producing better LOD.
102 In addition, we have optimized the fabrication process to make 44 chips simultaneously on a four-inch
103 wafer. The devices are tested using freshly collected waste-water samples to detect SARS-CoV-2 spike
104 protein, Influenza A hemagglutinin, RSV glycoprotein, and caffeine for comparison with lab-based WBE
105 methods.

106 2. Materials and Methods

107 2.1 Graphene Platform Development

108 2.1.1 Graphene as a transducer

109 Graphene is particularly useful yet challenging as a transducer due to its extreme sensitivity to
110 surface charges (Castro Neto et al. 2009; Ping et al. 2016a; Hwang et al. 2016). Nonetheless, graphene is
111 biocompatible and can be prepared at wafer scale. Due to its zero-band gap, it has a well-defined Dirac

112 point (charge neutrality point) where its valence and conduction bands meet. This produces a peak in
113 resistance when the chemical potential reaches the Dirac point (Fig. 1). When biomolecules attach to
114 the surface of the graphene, it is generally assumed charge is transferred to graphene either directly or
115 from conformational changes in the probe (J. Li et al. 2021; Seo et al. 2020a). This enables quantification of
116 the target concentration via a shift in voltage at which the Dirac point appears.

117 Another advantage of graphene is the ease of functionalization with the biomolecules used as
118 probes (Pinto, Gonçalves, and Magalhães 2013). These probes can be bonded to aromatic rings (e.g.,
119 Pyrene), which attach to the graphene through π - π stacking. This allows for tremendous
120 biocompatibility between graphene and a host of biomolecules without unintentional disorder from
121 chemical bonding. However, typically, graphene is functionalized via a two-step process, where the
122 linker molecule is attached using dimethylformamide (DMF), and then the probe is later bound to the
123 linker molecule (Seo et al. 2020b; Kwong Hong Tsang et al. 2019; https et al. 2022; Nekrasov et al. 2022).
124 Unfortunately, the DMF tends to react with the device, causing instability, higher LOD, and lower
125 reproducibility, and can attack polymers and passivation layers, degrading the device (Khan and Song
126 2021). As described later, we have avoided this issue and improved the LOD and reproducibility needed
127 for point-of-need WBE using probes pre-attached to the linker molecule and incubated in PBS.

128 Likewise crucial for detection in complex wastewater matrices, graphene is insensitive to the
129 sample medium's pH levels (Fu et al. 2011). We demonstrated this in our recent work on opioid
130 metabolite detection in wastewater (Kumar et al. 2022), in which we showed the simultaneous
131 detection of Noroxycodone, Norfentanyl, and EDDP (2-ethylidene-1, 5-dimethyl-3, 3-
132 diphenylpyrrolidine) with an LOD below that of HPLC-MS (Kumar et al. 2022). This work also exhibited
133 our platform's robustness and selectivity of the target molecules in wastewater. Unlike traditional field-
134 effect transistor (FET) sensors that require large gate voltages (>60V) (Ping et al. 2016a), we have

135 demonstrated our ionic liquid-gated GFETs are compatible with simple electronics requiring less than 2V
136 (Kumar, Gray, et al. 2020; Kumar, Wang, et al. 2020).

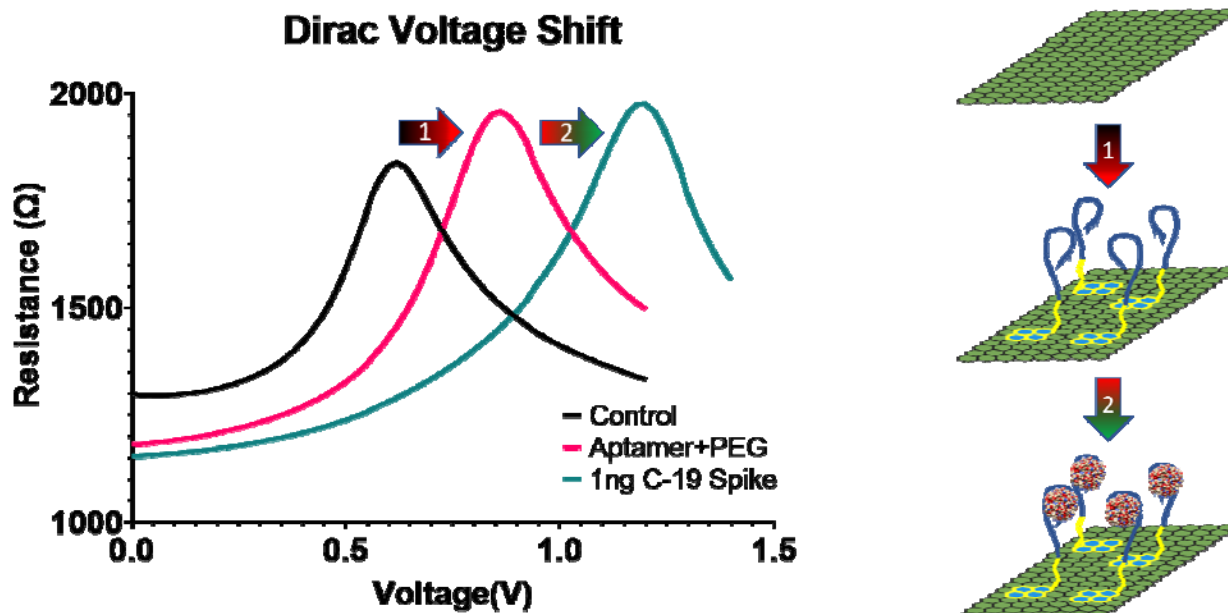


Fig. 1 – Dirac voltage shifting with aptamer and target attachment: The plot on the left shows the positive shift in the Dirac point (peak of the curves) from the intrinsic position of the bare graphene (black) of approximately 0.6V. After a 2:1 mixture of the aptamer probe to PEG is added the Dirac point shifts positively to about 0.8V (pink). A large shift in the Dirac point to 1.2V is then seen (green) in the presence of 1ng/ml of the target protein for SARS-CoV-2. On the right is a schematic of the bare graphene, aptamer attachment, and target attachment.

137 2.1.2 GFET Fabrication, Characterization, and Functionalization

138 To bring our GFET-based Graphene Electronic Multiplexed Sensor (GEMS) towards point-of-need
139 WBE, we modified our fabrication method and device design to enable production on a four-inch silicon
140 wafer (Fig. 2a – Top) before dicing into individual chips. This has drastically reduced our costs per chip
141 primarily due to a drastic decrease in fabrication time. Prior to wafer-scale fabrication, we were able to
142 produce 6 – 8 chips in four days. We can now produce 44 GEMS in the same amount of time. Each GEMS
143 has 20 GFETs arranged in groups of five for rapid statistical analysis of variability between GFET devices.
144 To enable multiplexed detection, the groups are segregated with PDMS wells with individual coplanar
145 side gates (Fig. 2b). This enables individual functionalization of each well with a different probe without
146 cross-functionalization.

147 We first pattern bottom contacts on a four-inch Si/SiO₂ wafer using bi-layer photoresist
148 (LOR1A/S1805) and photolithography followed by e-beam deposition of 5 nm of titanium wetting layer
149 and 20 nm of platinum. Platinum is chosen to minimize contact resistance to graphene because it is
150 robust and has low surface potential (Fujii, Kasuya, and Kurihara 2017). After metal liftoff, the contacts
151 were annealed under vacuum for 10 hours at 400°C to remove any remaining photoresist and increase
152 the electrodes' smoothness, allowing for better graphene attachment. CVD graphene was transferred on
153 top of the entire wafer by General Graphene Corp. in Knoxville, TN. The wafer was then annealed under
154 vacuum in the e-beam chamber for nine hours at 300°C to remove any remaining residues and water
155 from the transfer process. Before removing from the e-beam chamber, 3 nm of aluminum oxide (AlOx)
156 was deposited to protect the graphene from further chemicals and atmosphere during later fabrication
157 steps. Once removed, the wafer was baked on a hotplate in our glovebox at 175°C for five minutes to
158 ensure aluminum oxide adhesion. The same bi-layer resist process and photolithography system were
159 then used to pattern the graphene for etching via oxygen plasma. The MF-321 developer (from Kayaku)
160 used to develop the pattern after lithography has the added benefit of also removing the 3 nm of AlOx
161 from atop the graphene we wish to etch. This was followed by argon plasma to remove any oxide layer
162 formed on the platinum by the oxygen plasma on the coplanar side gate. Failing to remove this layer has
163 led to higher initial Dirac points and, in turn, lower sensitivity in our devices.

164 Next, the devices were cleaned with Remover PG and rinsed with IPA and DI water. The chips
165 were then baked under a vacuum at 200°C for one hour to remove any water and clean any residue
166 from the wafer. After this, a 50 nm passivation layer of aluminum oxide was deposited to encapsulate
167 the devices while the wafer was still hot. Oxygen was flowed to achieve a pressure of ~10⁵ Torr during
168 AlOx deposition to replenish oxygen stripped from the AlOx crystals during e-beam deposition. A final
169 single layer (S1805) photolithography step was then performed to expose the graphene sensing
170 windows (10um x 40um) and the contact pads for wire bonding. Exposed AlOx was then etched with

171 65:35 diluted TRANSECH-N (from Transene) for 14 minutes at 80°C, then rinsed with DI water. The
172 remaining photoresist was then removed with Remover PG and rinsed with IPA and DI water. The wafer
173 was then diced using a Pelco Wafer Dicing system, eliminating the need for a wafer dicing saw and its
174 associated chemicals. The chips were then mounted to chip carriers and wire-bonded. Following this,
175 PDMS wells made in-house with custom 3D-printed molds were placed on the chips to hold the

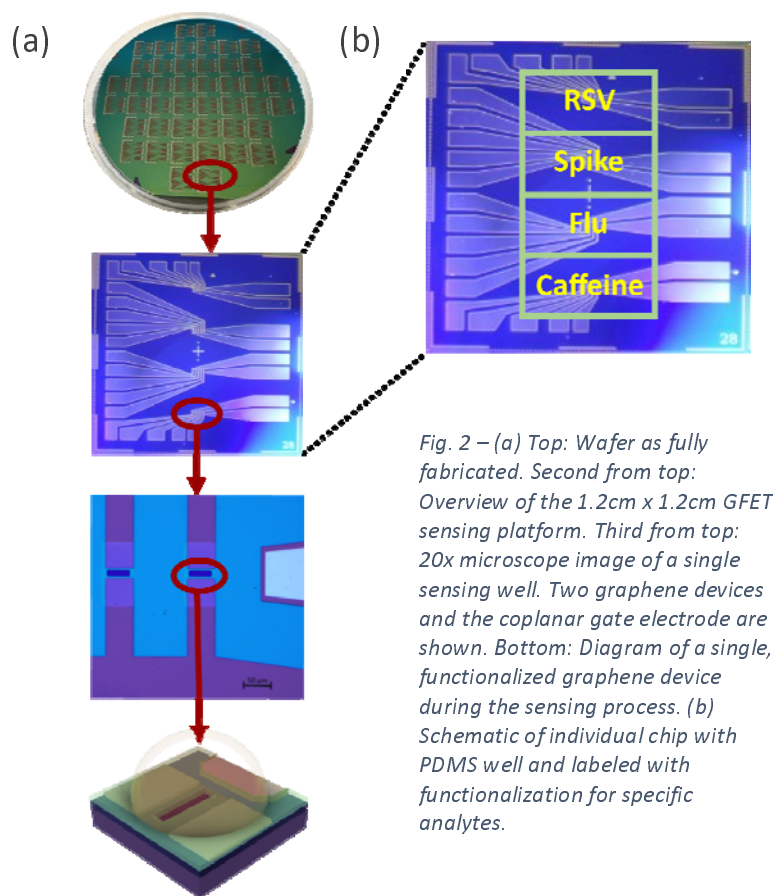


Fig. 2 – (a) Top: Wafer as fully fabricated. Second from top: Overview of the 1.2cm x 1.2cm GFET sensing platform. Third from top: 20x microscope image of a single sensing well. Two graphene devices and the coplanar gate electrode are shown. Bottom: Diagram of a single, functionalized graphene device during the sensing process. (b) Schematic of individual chip with PDMS well and labeled with functionalization for specific analytes.

176 functionalization liquids and target mixtures during incubation as per our sensing protocols.

177 2.2 Pre-Linked Aptamers

178 We employ aptamer probes due to their high affinity, stability, and small size (Cai et al. 2018;
179 Urmann et al. 2017). Aptamer-based protein biosensing depends on aptamer-target binding (Y. Wu et al.
180 2014), which several factors can complicate. Structurally complex protein targets have more binding
181 sites and interaction types than small molecules (S. Jones et al. 2001; Kohlberger and Gadermaier 2022).

182 This increase in complexity can result in aptamers with decreased target specificity if the experimental
183 design of SELEX is flawed (Qian et al. 2022). Generation of aptamers for proteins via SELEX is more
184 manageable for small molecules (Y. Wu et al. 2014), but the conformation of the protein (purified or
185 native) can alter or hinder aptamer binding (Zhou and Rossi 2017; Z. Zhang et al. 2021). Careful
186 consideration is necessary to ensure binding conditions mirror real-world binding conditions. With this
187 in mind, we chose the Universal Aptamer (UA) (Bhardwaj et al. 2019; Shiratori et al. 2014; C.-H. Wang,
188 Chang, and Lee 2016) for Influenza A hemagglutinin, H8 (Percze et al. 2017) for RSV, and 1C (Y. Zhang,
189 Juhas, and Kwok 2022) for SARS-CoV-2 spike proteins based on their binding affinities to their targets.
190 See the Supplemental for further information regarding the aptamers.

191 Generally, to attach the aptamer to graphene, the device is first incubated with 10 mM 1-
192 pyrenebutyric acid N-hydroxysuccinimide ester (PBASE) linker molecule dissolved in DMF for one hour.
193 After performing a Dirac point measurement to see the shift due to DMF and PBASE, a 2:1 mixture of
194 aptamer to polyethylene glycol (PEG) is incubated for one hour. Adding PEG to the probe mixture has
195 been widely employed (Szunerits et al. 2023; Rodrigues et al. 2022) to prevent unwanted attachment of
196 molecules to any unlinked PBASE molecules and provide space between aptamers, limiting their
197 interactions. The PEG also stabilizes the devices by minimizing drift and standard deviation between
198 different devices.

199 To further reduce cost, analysis, and fabrication time and boost reproducibility, we altered this
200 typical process by pre-attaching the aptamers and PEG to the PBASE molecules (See supplementary
201 information for more details regarding pre-linking.). Indeed, DMF is known to dope graphene (G. Wu et
202 al. 2017) and thus would be expected to result in a higher limit of detection. With this in mind, we
203 performed identical experiments with GEMS using the standard DMF attachment procedure and our
204 pre-linked PEG (PL-PEG) and probes (PL-aptamers). As seen in Fig. 3 and Table 1, more significant Dirac
205 point shifts occurring at much lower LODs are seen in devices with pre-linked (PL) probes. Lastly, to

206 ensure graphene cleanliness and device reproducibility, much of the fabrication was carried out in a
207 pure argon environment inside our cleanroom-in-a-glovebox (Gray et al. 2020).

208 2.3 Optimization in PBS

209 2.3.1 Viral aptamers

210 Selectivity and concentration analysis was first conducted in 1x PBS to determine the aptamer
211 viability without the background signal from wastewater. Specifically, the numerous constituent
212 components in wastewater (Henze, Mogens; van Loosdrecht, Mark; Ekama, George; Brdjanovic 2008; M.
213 H. Huang, Li, and Gu 2010; Novo et al. 2013), many of which are charged ions, can produce false
214 positives. For each target, we first determined the initial Dirac point of the graphene in 0.01x PBS (see
215 Supplemental). Diluted PBS minimizes the Debye screening effect (Stern 2007). Typically, we observe a
216 Dirac point around 0.6 V (± 0.1 V) due to the work function of the platinum side gate electrode (Fujii,
217 Kasuya, and Kurihara 2017). This baseline Dirac point ensures the graphene quality without unwanted
218 doping. This is further confirmed by the nearly symmetric slopes to the left (hole regime) and to the
219 right (electron regime) of the Dirac point, which results from the charge carrier mobilities (Gosling et al.
220 2021). Passivation issues are typically indicated by double peaks in the curves. Good passivation is also
221 confirmed by ensuring the Dirac point does not drift with repeated gate voltage sweeps. The highest
222 quality devices have an initial Dirac point in the range of 0.58 – 0.7 V with an average starting resistance
223 around 2000 Ω and a stable Dirac point after three measurements. Data on initial Dirac point and
224 starting resistances were collected for 545 different GFETs fabricated over two years in our lab, showing
225 that most of our devices fall within these parameters (see Supplemental).

226 After initial testing, we incubated the graphene devices for one hour with a 2:1 mixture of 10uM
227 PL-aptamer to 10uM PL-PEG, which was optimized in our previous work with opioids in wastewater and
228 oral disease biomarkers in saliva (Kumar, Wang, et al. 2020; Kumar, Gray, et al. 2020; Kumar et al. 2022).

229 Dirac point measurements are again conducted in 0.01x PBS to confirm attachment to the graphene
230 surface. Upon attachment, the charged phosphate backbone of the aptamer induces positive charge
231 carriers into the graphene, producing a positive 150-200mV shift in the Dirac point (see Supplemental).
232 Atomic force microscopy and Raman measurements have also been performed to confirm the
233 attachment (see Supplemental).

234 We first assessed all aptamer selectivity against a negative control. For example, the Influenza A
235 hemagglutinin (HA) with a concentration of 10 – 100 ng/ml that is far beyond that found in wastewater
236 (tens of pg/ml), is incubated on the devices for one hour in the well containing the SARS-COV-2 SPIKE
237 PROTEIN aptamer (1C). No shift in the Dirac point was seen, showing the HA protein does not bind to
238 the 1C aptamer (Fig. 3 – Covid). Similar negative control analyses were conducted in the wells
239 functionalized with the Influenza and RSV aptamers. As shown in Fig. 3, these aptamers had a slightly
240 higher non-specific interaction with the negative control proteins. Nonetheless, the Dirac point shifts in
241 wells with the Influenza and RSV aptamers resulting from negative controls were relatively small
242 (approximately 50 mV), setting the baseline for future measurements.

243 Next, we focused on assessing each aptamer's limit of detection and affinity. We followed a
244 standard protocol of incubating the devices with a specific concentration of the target proteins. After
245 incubation, the device is rinsed with 1x PBS and DI water before performing the Dirac point
246 measurement in 0.01x PBS. For each concentration, the reported shift is the difference in the Dirac point
247 value obtained from that of the negative control. After measuring the Dirac shift, we incubated with
248 increasing target protein concentrations. To ensure the absence of systematic errors, we have also
249 performed measurements with random concentrations to ensure they match the signal detected by a
250 systematic increase in concentration.

251 Beginning with low concentration, each incubation is conducted for one hour. We found that
252 concentrations below 1 fg/ml for the SARS-COV-2 spike protein did not change the Dirac point.
253 However, the RSV and HA proteins produced shifts at much lower concentrations (approximately 10
254 ag/ml). This shift discrepancy may be due to the newness of the SARS-COV-2 spike aptamer and future
255 improvements can improve its binding affinity. The average shift from all devices in the well and their
256 standard deviations are plotted in the same graph as the negative control's shift. The concentrations are
257 increased by one order of magnitude in each subsequent incubation, and the same rinsing and sensing

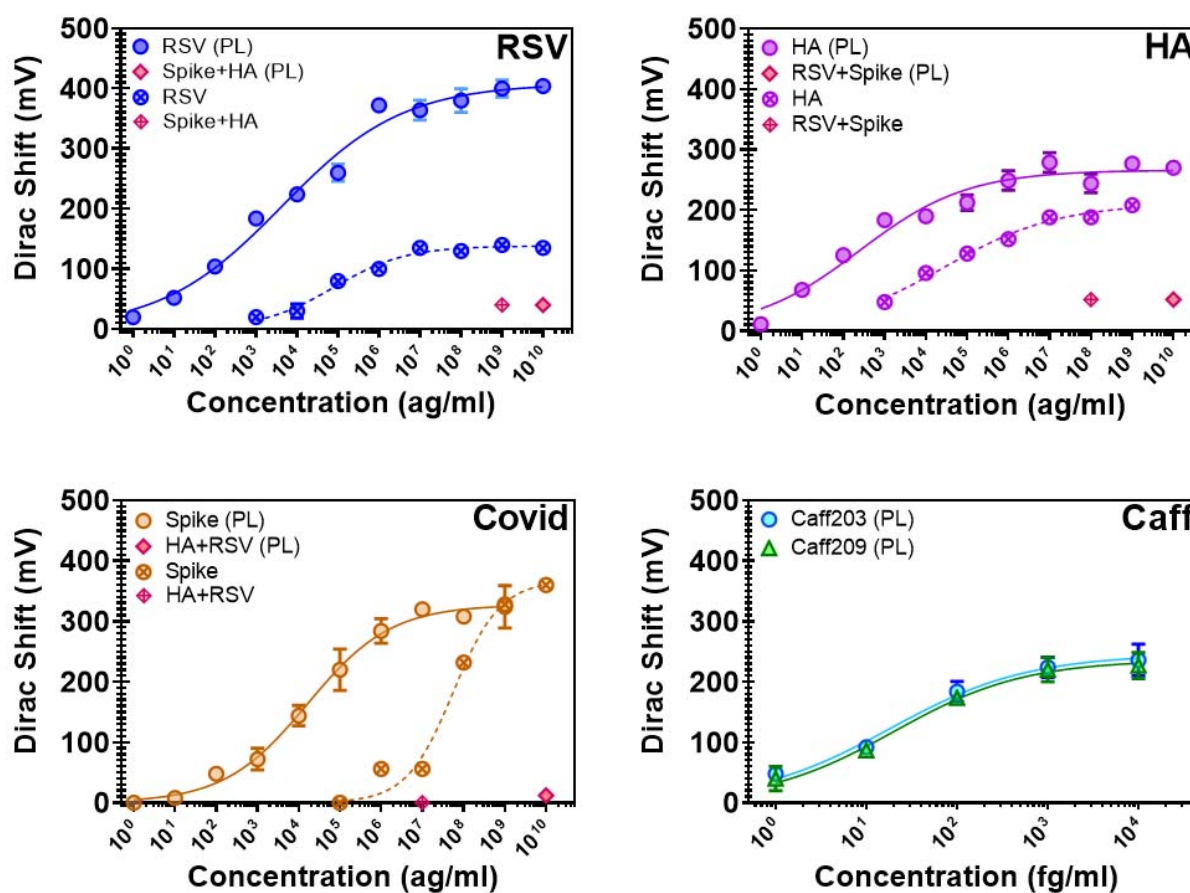


Fig. 3 –Concentration dependance measurements of viral proteins in PBS. Error bars calculated from the five GFETs per sensing well. Data points with crosses and dashed curves indicate non-pre-linked aptamers were used. Top Left - Influenza A Hemagglutinin detection. High concentrations of RSV and COVID Spike proteins used as a negative control. (PL) denotes pre-linked aptamer experiment. Top Right and Bottom Left - Same as in HA plot but with SARS-CoV-2 Spike and RSV proteins, respectively. Non-target proteins used as negative control in each case. Bottom Right - Concentration dependence measurements of two caffeine aptamers. Caffeine measurements were only conducted with pre-linked aptamers.

258 protocol is conducted for each. The concentrations are increased until a saturation point is reached,
259 determined by no further shift with two consecutive high concentrations.

260 Upon collecting the concentration dependence, we found the binding characteristics of the
261 aptamer by fitting the Dirac voltage shift versus target analyte concentration to Hill's equation (Goutelle
262 et al. 2008):

$$V_D = \frac{V_D^{max} * C^n}{K_D^n + C^n} \quad (1)$$

263 Here, V_D is the Dirac voltage shift measured in mV, V_D^{max} is the maximum Dirac voltage shift at the
264 saturation point, C is the concentration of the target analyte, n is the Hill Coefficient
265 determined to be the maximum slope on a log plot of the response curve, and K_D is the
266 dissociation constant. The parameters were found using a least squares fit model in Matlab
267 after providing estimates of the Hill Coefficient, maximum Dirac voltage, and dissociation
268 constant. Due to the five devices in each well of the GFET, we can perform statistical analysis
269 immediately. This allows us to calculate the LOD for each analyte by using the residuals of the
270 standard deviation against the Hill fit using 3σ analysis (Belter, Sajnóg, and Barańkiewicz 2014):

$$LOD = \frac{3\sigma}{n} \quad (2)$$

271 Here, σ is the standard deviation from the fit and n is again the Hill slope. This was used to find the LODs
272 in Table 1.

Table 1 Comparison of LODs between pre-linked and unlinked aptamers for each target analyte in PBS. All pre-linked virus experiments were conducted on a single GFET chip and unlinked on another. Caffeine experiments were only performed with pre-linked aptamers and done on a single GFET chip.

| Target | Unlinked Aptamer | Pre-Linked Aptamer |
|-------------------------------------|------------------|--|
| SARS-CoV-2 Spike Protein | 91 pg/ml | 55 ag/ml |
| Hemagglutinin (Flu A) | 79 fg/ml | 408 ag/ml |
| Respiratory Syncytial Virus Protein | 43 fg/ml | 453 ag/ml |
| Caffeine | N/A | Caff203: 35 fg/ml Caff209: 26 fg/ml |

273

274 2.3.2 Caffeine aptamer

275 WBE programs use several different biomarkers to determine the total contributing population.

276 These include caffeine, paraxanthine (caffeine's metabolite), creatine, 5-hydroxyindoleacetic acid (5-

277 HIAA, serotonin metabolite), and pepper mild mottle virus (PMMoV) given their ubiquitousness in

278 human diets and survivability in wastewater (Hsu et al. 2022). Paraxanthine and PMMoV concentration,

279 in particular, are excellent means for population normalization (C. Li et al. 2022b). Unfortunately, to the

280 best of our knowledge, no aptamer has yet been developed for PMMoV or paraxanthine. Therefore, to

281 test our platform's capabilities as a means for population normalization in wastewater, two previously

282 reported caffeine aptamers were selected based on their reported results that show micromolar

283 sensitivity in human serum (P. J. J. Huang and Liu 2022), two of which (Caff203 and Caff209) were

284 chosen for our tests in wastewater. Both the Caff203 and Caff209 aptamers were pre-attached to the

285 PBASE linker molecules, and the same functionalization and sensing protocols were followed as the virus

286 proteins. Both were evaluated first in PBS to determine their viability before exposure to wastewater.

287 Caff203 was found to have an LOD of 35 fg/ml in PBS, while Caff209 showed 26 fg/ml in PBS (Fig. 3). Due

288 to its lower LOD, Caff209 was selected for future experiments.

289 3. Results

290 3.1 Wastewater biosensing

291 3.1.1 Wastewater dilution optimization

292 Next, we turned to testing GEMS with wastewater. In our earlier work on opioid metabolites, we
293 found diluting the wastewater with 1x PBS to a 20:1 mixture necessary to minimize unwanted Dirac
294 point shifts and false positives from the myriad components and non-neutral pH (6-9). Given the
295 improved device performance with pre-attachment, we re-optimized this dilution to attempt a lower
296 LOD. We began by incubating the 1C PL-aptamer and PL-PEG, as previously discussed. The wastewater
297 was then passed through a 0.3-micron filter to remove large particulates. Next, various dilutions (2:1,
298 5:1, 10:1, and 20:1) were incubated directly on the devices for one hour, and the resulting Dirac point
299 shift is shown in Fig. 4. We found the 10x dilution caused an approximate 60 mV Dirac point shift, the
300 same as the 20x dilution. Since PBS does not induce a shift, the background signal from wastewater will
301 increase the LOD by setting a floor below which we cannot uniquely detect the target, as indicated by
302 the horizontal dashed lines in Fig. 5. Next, four samples were diluted with the 2:1, 5:1, 10:1, and 20:1

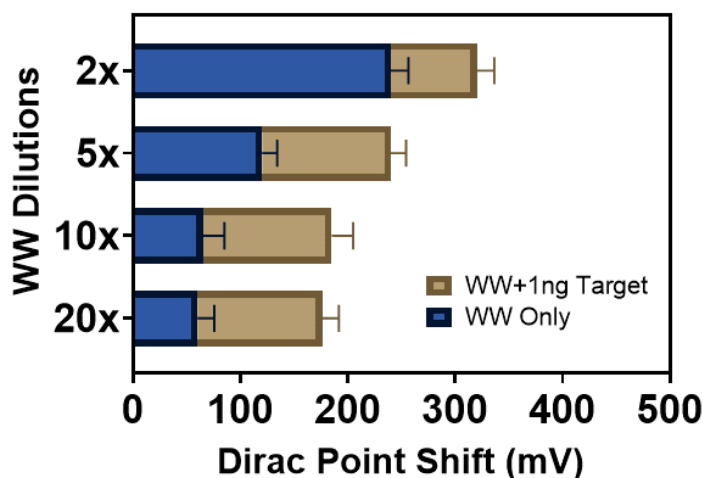


Fig. 4 – Histogram of the average Dirac point shift at various wastewater dilutions. The blue areas show the average Dirac point shift for five GFET devices after incubation of diluted wastewater for one hour. The tan areas show the further Dirac point shift after incubating the GFETs for one hour with 1ng/ml of target protein in their respective wastewater dilutions.

303 PBS to wastewater samples to create 1 ng/ml solutions of SARS-COV-2 spike protein and incubated on
304 the devices for one hour. This was done to determine if wastewater dilution affected the ability of the
305 aptamers to find the target proteins. The 1 ng/ml concentration was used since this is the point at which
306 the SARS-COV-2 SPIKE PROTEIN aptamer saturated when tested in 1x PBS. Interestingly, there was a
307 statistically insignificant difference in the shift between the 10:1 and 20:1 wells. Both measured a shift
308 of around 130 mV after incubating with the spike protein mixture. Thus, we focused 10:1 PBS to
309 wastewater dilution to achieve the smallest possible LOD in wastewater.

310 3.1.2 Detection of Analytes in Wastewater

311 Having optimized the wastewater dilution, we performed a similar series of concentration-dependent
312 measurements with the same protocol done first in PBS. The experiments were conducted in two
313 rounds for each analyte. Experiments were first performed on a single GFET chip. Four wells were
314 functionalized with a different pre-attached aptamer: 1C for SARS-CoV-2, UA for hemagglutinin, H8 for
315 RSV, and Caff209 for caffeine. A fresh wastewater sample was obtained (collected one day prior and
316 stored a 4°C overnight), filtered, and diluted in a 10:1 ratio with PBS and spiked with virus proteins and
317 caffeine to make concentrations ranging from 1 fg/ml to 1 ng/ml with an increase of one order of
318 magnitude between each concentration. The second round of experiments was conducted one month
319 later using a newly fabricated GFET chip, fresh pre-attached aptamers, and a new wastewater sample. In
320 both instances, the negative controls were tested first at 1 ng/ml to check selectivity, followed by
321 increasing the concentrations of the target analyte. In both rounds, the negative controls showed little
322 to no shift beyond the background 60mV shift from the wastewater (dashed lines in Fig. 5).

323 The resulting concentration curves are shown in Fig. 5, and LODs for each round are shown in
324 Table 2. As expected, LOD values increased over the PBS results due to the intrinsic 60mV signal from
325 the wastewater. Nonetheless, the larger LODs are all well within the range for the concentrations of

326 each analyte in wastewater. SARS-CoV-2 has been shown to contain 24 ± 9 spike proteins per virion (Ke et
327 al. 2020), theoretically suggesting the LOD for our GEMS platform to be on the order of 27 – 59
328 virions/ml (27,000 – 59,000 virions/L) in wastewater assuming fully lysed virions. Influenza A has been
329 found to contain 300 – 400 HA proteins per virion (Einav, Gentles, and Bloom 2020), giving a theoretical
330 LOD of fully lysed virions in the 1.5 – 7 virions/ml (1,500 – 7000 virions/L). To the best of our knowledge,
331 the average number of proteins for RSV has not yet been determined. Assuming a similar number
332 between the spike and the Influenza A proteins, the theoretical, fully lysed RSV virions could be 15 – 397
333 virions/ml (15,000 – 397,000 virions/L). Like the experiments conducted in PBS, the RSV and SARS-COV-2
334 spike aptamers show little to no shift with the high concentration of negative control. In contrast, the
335 HA aptamer showed a small but significant shift of around 60 mV with negative control. This could be
336 partly due to UA's longer length compared to the others, allowing it to bind to more constituent
337 elements in the wastewater. It could also be due to HA proteins already present in the wastewater
338 sample, which was collected during the 2022 – 2023 Flu season.

339 Due to its lower LOD found in PBS (Table 1), Caff209 was selected for analysis in wastewater.
340 Interestingly, the LOD in wastewater was lower than in PBS, which was not seen with the virus proteins.
341 This could be due in part to the salt content in wastewater facilitating binding (Lores and Pennock 1998)
342 of the much smaller caffeine molecules, which are 0.194 kDa as compared to the larger proteins having
343 sizes of 139.7 kDa, 59 kDa, and 37 kDa for spike, HA, and RSV respectively, lowering the variability
344 between the devices.

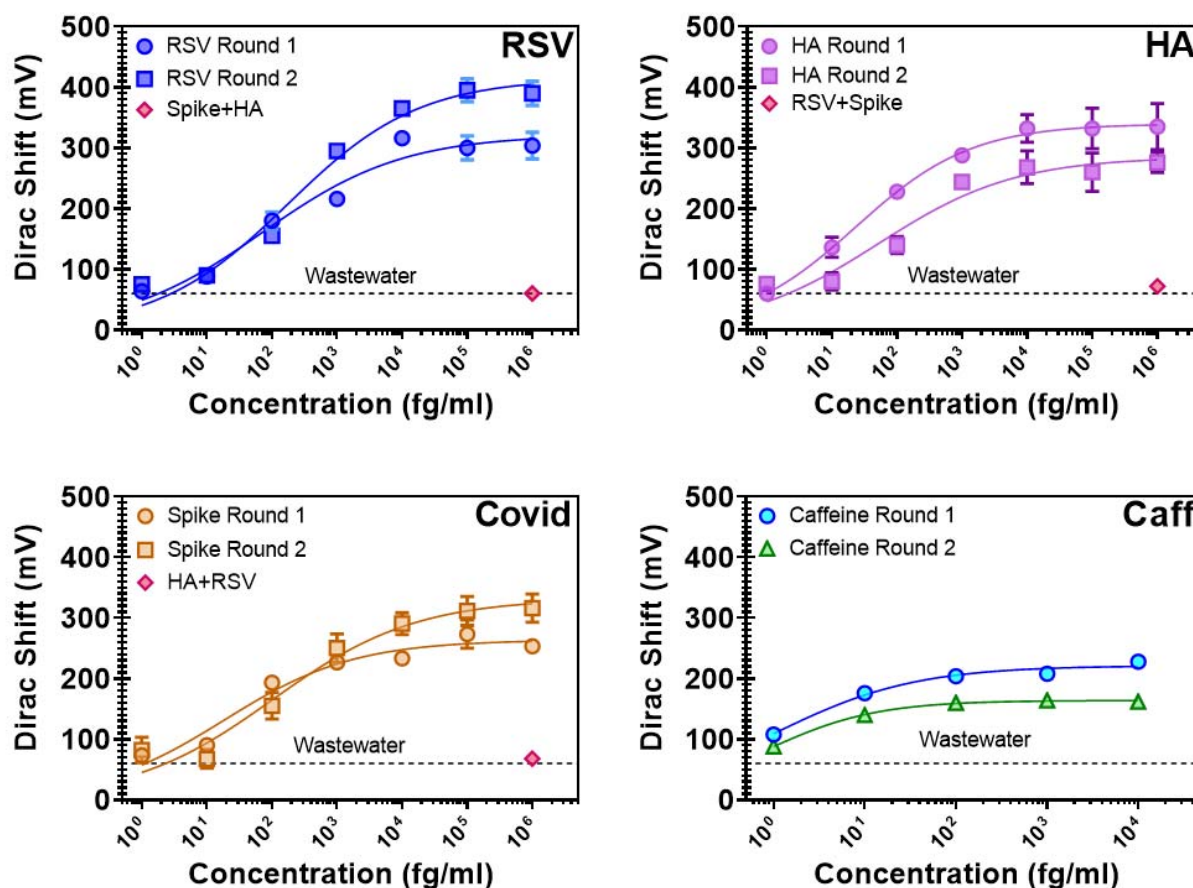


Fig. 5 – Concentration dependence measurements of viral proteins and caffeine in wastewater. Error bars calculated from the five GFETs per sensing well. From left to right, HA, RSV, and COVID spike proteins and Caffeine. Horizontal dashed line shows intrinsic background shift from the wastewater itself.

345 To put these LODs in context, we compare them with other reported LODs. BioBot reports a
 346 limit of detection (LOD) for SARS-CoV-2 of 9000 copies/L using RT-qPCR (Biobot 2023a) (approximately
 347 10 whole virions/L), which is lower than concentrations typically found in wastewater. The reliance on
 348 lab testing results from these low virus loads in wastewater requires amplification and/or viral
 349 concentration steps to detect. These concentrations can range from, in the case of SARS-CoV-2, 150,000
 350 – 141.5 million viral genome copies (150 – 141,500 whole virions (Sender et al. 2020)) per liter of
 351 wastewater (Hart and Halden 2020). Influenza A concentrations are reported to be around 260,000
 352 copies per liter (Heijnen and Medema 2011) and RSV 1,071 – 70,700 copies per liter (Ahmed et al. 2023).
 353 Others have reported LODs from RT-qPCR as low as 2.9 – 4.6 copies per reaction after concentrating the

354 sample from 50ml to 20ul (Ahmed et al. 2022). Several studies have found levels of shed virus can vary
355 substantially depending on patient infection level and virus variants, ranging from $10^2 - 10^7$ copies/ml
356 (D. L. Jones et al. 2020; Pan et al. 2020; Zang et al. 2020; Han et al. 2020). These levels will significantly
357 decrease upon reaching a wastewater treatment facility due to dilution and virus decay, highlighting the
358 need for more localized collection and analysis. While our GEMS platform cannot achieve the low LODs
359 seen with RT-qPCR, its LODs are 1 – 2 orders of magnitude lower than what has been reported with LC-
360 MS (Table 2).

Table 2

Limits of Detection (LOD) for each target analyte from two separate experimental rounds. Each round was conducted on a single GFET chip. Based on their average molecular weights, LODs were converted from fg/ml to proteins/ml.

| Target | Round 1 LOD | Round 2 LOD | Reported LC-MS from Literature |
|--|---|--|--|
| SARS-CoV-2 Spike Protein | 136 fg/ml (890 proteins/ml) | 187 fg/ml (1224 proteins/ml) | $10^5 - 10^6$ copies/ml (Griffin and Downard 2021; Dollman, Griffin, and Downard 2020; Nikolaev et al. 2020; Picó and Barceló 2021) (~3000 fg/ml) |
| Hemagglutinin (Flu A) | 39.6 fg/ml (612 proteins/ml) | 181 fg/ml (2799 proteins/ml) | 7×10^6 copies/ml (Bojórquez-Velázquez et al. 2022) (~30,000 fg/ml) |
| Respiratory Syncytial Virus glycoprotein | 176 fg/ml (5927 proteins/ml) | 175.4 fg/ml (5959 proteins/ml) | 3.6×10^7 copies/ml (Bojórquez-Velázquez et al. 2022) (~40,000 fg/ml) |
| Caffeine | 10 fg/ml (3.1×10^7 molecules/ml) | 2 fg/ml (6.2×10^6 molecules/ml) | 5000 fg/ml (Huerta-Fontela, Galceran, and Ventura 2007) |

361

362 In the case of LC-MS, LODs between $10^5 - 10^6$ copies per nasopharynx sample (Dollman, Griffin,
363 and Downard 2020; Nikolaev et al. 2020) have been reported. While LC-MS has been used to detect
364 SARS-CoV-2 in wastewater (Peng et al. 2022; Lara-Jacobo et al. 2022), no detection limit has yet to be
365 reported. So-called “rapid tests,” on the other hand, while having short analysis time, typically rely on
366 LFIA, which to the best of our knowledge have not shown the ability to rapidly sense the low level of
367 virus in unprocessed wastewater. An LFIA sensed human adenovirus in processed wastewater by first
368 concentrating the wastewater sample through PEG precipitation overnight and then performing a
369 recombinase polymerase amplification step and achieving an LOD of 50 copies/reaction starting from an
370 initial sample size of 1L (Rames and Macdonald 2019). While this is a low LOD, the tradeoff is in the time
371 and complexity of the analysis.

372 3.2 Blind Testing

373 To ensure device integrity, a blind test in wastewater was performed. A single chip was
374 functionalized with each virus aptamer in a different well. Four concentrations of each target protein
375 were made by one author (O.R.P.) and were coded with a four-digit number (1738, 1993, 2930) with no
376 indication of the contents. These were tested by another author (M.G.) using the same sensing protocol
377 outlined above to determine which coded sample contained each protein. As shown in Fig. 6, for
378 concentrations above 100 pg/mL (consistent with our earlier LOD) the target can easily be identified by
379 only producing a Dirac shift in one well. Based on this, M.G. identified each target, which was confirmed

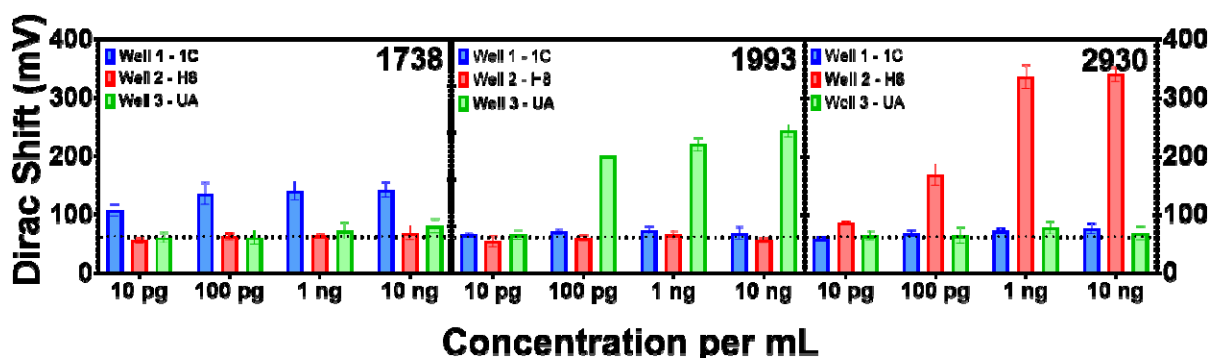


Fig. 6 – Wastewater Blind Tests: Each plot represents the differing concentrations for a coded sample. The assorted colors indicate the aptamer used in each well; blue for the 1C (Covid), red for H8 (RSV), and green for UA (Flu). The horizontal dotted line is the intrinsic shift from the wastewater. M.G. found that 1738 was COVID spike proteins (left), 1993 was HA (middle), and 2930 was RSV. Each was confirmed by O.R.P.’s written records.

380 correct by O.R.P.'s written records.

381 4. Conclusions and Future Work

382 To summarize, we showed the viability of our GEMS platform for selective, specific,
383 simultaneous, and highly sensitive detection of four different analytes in wastewater, including caffeine
384 for population normalization and three different viral proteins. We achieved limits of detection (see
385 Table 1) one to two orders of magnitude better than HPLC-MS (Fig. 5) (Dollman, Griffin, and Downard
386 2020; Nikolaev et al. 2020; Peng et al. 2022; Lara-Jacobo et al. 2022; Kasprzyk-Hordern et al. 2023;
387 Mestankova et al. 2012) and below the levels needed for effective early interventions (Peng et al. 2022).
388 Results are obtained using a 1 cm² chip in just over one hour with minimal human intervention and
389 without bulky, expensive lab equipment or costly reagents. Simple wastewater preparation can be easily
390 performed with minimal training, while low voltage and resistance ranges can be operated with simple
391 and cheap electronics. The cost is minimized by wafer-scale fabrication and pre-linked aptamers, further
392 enhancing reproducibility and LOD. Combined with our previous results, the scalable GEMS platform
393 enables rapid, easy, and cheap wastewater sensing of a wide range of analytes (opioid metabolites,
394 viruses, etc.). This shows our platform to be a practical choice for wastewater-based epidemiology for
395 viral testing and can lead to finding hotspots for future virus outbreaks. Our platform's low cost and
396 power requirements could allow WBE to be performed on a building-by-building level in low-resource or
397 rural settings, ushering in a new era of wastewater testing. Enabling this will require future efforts for
398 on-chip electronics and microfluidics for sample preparation and a more comprehensive array of
399 analytes to be tested on the same chip.

400 Author Information

401 Corresponding Author

402 Kenneth S. Burch – Department of Physics, Boston College, Chestnut Hill, Massachusetts 02467, United
403 States; orcid.org/0000-0002-7541-0245; Email: ks.burch@bc.edu

404 Authors

405 Michael Geiwitz – Department of Physics, Boston College, Chestnut Hill, MA 02467, United States;
406 orcid.org/0009-0000-7197-9381

407 Owen Rivers Page – Department of Biology, Boston College, Chestnut Hill, Massachusetts 02467, United
408 States; orcid.org/0000-0003-4072-8509

409 Tio Marelo – Department of Physics, Boston College, Chestnut Hill, MA 02467, United States

410 Narendra Kumar – GRIP Molecular Technologies, Inc., 1000 Westgate Drive, Saint Paul, MN 55114;
411 orcid.org/0000-0002-5319-1547

412 Stephen Hummel – Department of Chemistry and Life Science, United States Military Academy, West
413 Point, NY 10996, USA

414 Vsevolod Belosevich – Department of Physics, Boston College, Chestnut Hill, MA 02467, United States

415 Qiong Ma – Department of Physics, Boston College, Chestnut Hill, MA 02467, United States

416 Tim van Opijnen – Department of Biology, Boston College, Chestnut Hill, Massachusetts 02467, United
417 States

418 Bruce Batten – GRIP Molecular Technologies, Inc., 1000 Westgate Drive, Saint Paul, MN 55114

419 Michelle M. Meyer – Department of Biology, Boston College, Chestnut Hill, Massachusetts 02467,
420 United States; orcid.org/0000-0001-7014-9271

421 CRediT authorship contribution statement

422 K.S.B., M.G., and N.K. conceived the project and designed the experiments. M.G. fabricated,
423 functionalized, and tested all GFET platforms. M.G., N.K., S.H, T.v.O., and K.S.B. selected all aptamers
424 and analyzed the data. O.R.P. pre-linked all aptamers with PBASE linker molecules. T.M. aided in the
425 design and placement of PDMS wells. S.H. validated 1C aptamer with flow cytometry. V.B. performed
426 AFM and wire bonding machine maintenance. Q.M. supervised AFM and wire bonding maintenance.

427 T.v.O. supervised flow cytometry. M.M. supervised aptamer pre-linking and blind test sample
428 preparation. B.B. and K.S.B. aided in data analysis. M.G., O.R.P., and K.S.B. wrote the manuscript.

429 Data Availability

430 All data is available on request.

431 Acknowledgements

432 The work of M.G., T.M., and K.S.B. are grateful for the support of the National Science Foundation (NSF)
433 EPMD program via grant 2211334. M.M.M., K.S.B. and O.P are grateful for support from the Boston
434 College Schiller Institute for Integrated Science and Society Exploratory Collaborative Scholarship grant.
435 M.G. would like to thank the Boston College Cleanroom & Nanofabrication Facility's staff, Stephen
436 Shepard and Dr. Chris Gunderson. M.G. and K.S.B. also thank Dr. Catherine Hoar for her insights on WBE.
437 We would also like to thank Mr. Bryan Horsely, Mr. George Heufelder, and Dr. Sara Wigginton from
438 MASSTC for providing wastewater samples and analysis of their source wastewater contents. Q.M. and
439 V.B. acknowledge the American Chemical Society Petroleum Research Fund (PRF) 66299-DNI10.

440 References

- 441 Adams, Grace. 2020. "A Beginner's Guide to RT-PCR, QPCR and RT-QPCR." *The Biochemist* 42 (3): 48–53.
442 <https://doi.org/10.1042/BIO20200034>.
- 443 Adelodun, Bashir, Fidelis Odedishemi Ajibade, Rahmat Gbemisola Ibrahim, Hashim Olalekan Bakare, and
444 Kyung Sook Choi. 2020. "Snowballing Transmission of COVID-19 (SARS-CoV-2) through
445 Wastewater: Any Sustainable Preventive Measures to Curtail the Scourge in Low-Income
446 Countries?" *Science of the Total Environment* 742: 140680.
447 <https://doi.org/10.1016/j.scitotenv.2020.140680>.
- 448 Ahmed, Warish, Nicola Angel, Janette Edson, Kyle Bibby, Aaron Bivins, Jake W. O'Brien, Phil M. Choi, et
449 al. 2020. "First Confirmed Detection of SARS-CoV-2 in Untreated Wastewater in Australia: A Proof
450 of Concept for the Wastewater Surveillance of COVID-19 in the Community." *Science of the Total
451 Environment* 728: 138764. <https://doi.org/10.1016/j.scitotenv.2020.138764>.
- 452 Ahmed, Warish, Aaron Bivins, Mikayla Stephens, Suzanne Metcalfe, Wendy J M Smith, Kwanrawee
453 Sirikanchana, Masaaki Kitajima, and Stuart L Simpson. 2023. "Occurrence of Multiple Respiratory
454 Viruses in Wastewater in Queensland, Australia: Potential for Community Disease Surveillance."
455 *Science of the Total Environment* 864: 161023. <https://doi.org/10.1016/j.scitotenv.2022.161023>.

- 456 Ahmed, Warish, Wendy J.M. Smith, Suzanne Metcalfe, Greg Jackson, Phil M. Choi, Mary Morrison,
457 Daniel Field, et al. 2022. "Comparison of RT-QPCR and RT-DPCR Platforms for the Trace Detection
458 of SARS-CoV-2 RNA in Wastewater." *ACS ES and T Water* 2 (11): 1871–80.
459 https://doi.org/10.1021/ACSESTWATER.1C00387/ASSET/IMAGES/LARGE/EW1C00387_0001.JPEG.
- 460 Belter, Magdalena, Adam Sajnóg, and Danuta Barańkiewicz. 2014. "Over a Century of Detection and
461 Quantification Capabilities in Analytical Chemistry-Historical Overview and Trends."
462 <https://doi.org/10.1016/j.talanta.2014.05.018>.
- 463 Bhardwaj, Jyoti, Narendra Chaudhary, Hajin Kim, and Jaesung Jang. 2019. "Subtyping of Influenza A
464 H1N1 Virus Using a Label-Free Electrochemical Biosensor Based on the DNA Aptamer Targeting the
465 Stem Region of HA Protein." <https://doi.org/10.1016/j.aca.2019.03.005>.
- 466 Biobot. 2023a. "FAQ - Technical Questions: Results – Biobot Analytics." 2023.
467 <https://support.biobot.io/hc/en-us/articles/360052012934-FAQ-Technical-Questions-Results>.
- 468 ———. 2023b. "FAQ - Variant Sequencing – Biobot Analytics." 2023. [https://support.biobot.io/hc/en-](https://support.biobot.io/hc/en-us/articles/14910772709527-FAQ-Variant-Sequencing)
469 [us/articles/14910772709527-FAQ-Variant-Sequencing](https://support.biobot.io/hc/en-us/articles/14910772709527-FAQ-Variant-Sequencing).
- 470 Bojórquez-Velázquez, Esaú, Miriam Livier Llamas-García, José M. Elizalde-Contreras, Jesús Alejandro
471 Zamora-Briseño, and Eliel Ruiz-May. 2022. "Mass Spectrometry Approaches for SARS-CoV-2
472 Detection: Harnessing for Application in Food and Environmental Samples." *Viruses* 2022, Vol. 14,
473 Page 872 14 (5): 872. <https://doi.org/10.3390/V14050872>.
- 474 Cai, Shundong, Jianhua Yan, Hongjie Xiong, Yanfei Liu, Dongming Peng, and Zhenbao Liu. 2018.
475 "Investigations on the Interface of Nucleic Acid Aptamers and Binding Targets." *Analyst* 143 (22):
476 5317–38. <https://doi.org/10.1039/C8AN01467A>.
- 477 Castro Neto, A H, F Guinea, N M R Peres, K S Novoselov, and A K Geim. 2009. "The Electronic Properties
478 of Graphene." <https://doi.org/10.1103/RevModPhys.81.109>.
- 479 CDC. 2023. "Update on RSV and New Vaccine Recommendation | CDC." 2023.
480 <https://www.cdc.gov/respiratory-viruses/whats-new/rsv-update-2023-09-22.html>.
- 481 Champredon, David, and Peter A. Vanrolleghem. 2023. "Editorial: Wastewater-Based Epidemiological
482 Surveillance of Respiratory Pathogens." *Frontiers in Public Health* 11.
483 <https://doi.org/10.3389/FPUBH.2023.1328452>.
- 484 Dollman, Nicholas L., Justin H. Griffin, and Kevin M. Downard. 2020. "Detection, Mapping, and
485 Proteotyping of SARS-CoV-2 Coronavirus with High Resolution Mass Spectrometry." *ACS Infectious*
486 *Diseases* 6 (12): 3269–76. <https://doi.org/10.1021/ACSINFECDIS.0C00664>.
- 487 Dong, Yongliang, Alex Lee, Deependra Kumar Ban, Kesong Wang, and Prabhakar Bandaru. 2023.
488 "Femtomolar Level-Specific Detection of Lead Ions in Aqueous Environments, Using Aptamer-
489 Derivatized Graphene Field-Effect Transistors." *ACS Applied Nano Materials* 6 (3): 2228–35.
490 https://doi.org/10.1021/ACSANM.2C05542/ASSET/IMAGES/LARGE/AN2C05542_0005.JPEG.
- 491 Einav, Tal, Lauren E Gentles, and Jesse D Bloom. 2020. "SnapShot: Influenza by the Numbers." *Cell* 182.
492 <https://doi.org/10.1016/j.cell.2020.05.004>.
- 493 Else, Laura, Victoria Watson, John Tjia, Andrew Hughes, Marco Siccardi, Saye Khoo, and David Back.
494 2010. "Validation of a Rapid and Sensitive High-Performance Liquid Chromatography-tandem
495 Mass Spectrometry (HPLC-MS/MS) Assay for the Simultaneous Determination of Existing and

- 496 New Antiretroviral Compounds." *Journal of Chromatography B* 878: 1455–65.
497 <https://doi.org/10.1016/j.jchromb.2010.03.036>.
- 498 Fu, Wangyang, Cornelia Nef, Oren Knopfmacher, Alexey Tarasov, Markus Weiss, Michel Calame, and
499 Christian Schönenberger. 2011. "Graphene Transistors Are Insensitive to PH Changes in Solution."
500 *Nano Letters* 11 (9): 3597–3600.
501 https://doi.org/10.1021/NL201332C/SUPPL_FILE/NL201332C_SI_001.PDF.
- 502 Fujii, Sho, Motohiro Kasuya, and Kazue Kurihara. 2017. "Characterization of Platinum Electrode Surfaces
503 by Electrochemical Surface Forces Measurement." *Journal of Physical Chemistry C* 121 (47): 26406–
504 13. <https://doi.org/10.1021/ACS.JPCC.7B09301>.
- 505 Gao, Ning, Teng Gao, Xiao Yang, Xiaochuan Dai, Wei Zhou, Anqi Zhang, and Charles M. Lieber. 2016.
506 "Specific Detection of Biomolecules in Physiological Solutions Using Graphene Transistor
507 Biosensors." *Proceedings of the National Academy of Sciences of the United States of America* 113
508 (51): 14633–38. [https://doi.org/10.1073/PNAS.1625010114/-](https://doi.org/10.1073/PNAS.1625010114/-/DCSUPPLEMENTAL/PNAS.201625010SI.PDF)
509 [/DCSUPPLEMENTAL/PNAS.201625010SI.PDF](https://doi.org/10.1073/PNAS.201625010SI.PDF).
- 510 Gosling, Jonathan H., Oleg Makarovskiy, Feiran Wang, Nathan D. Cottam, Mark T. Greenaway, Amalia
511 Patané, Ricky D. Wildman, Christopher J. Tuck, Lyudmila Turyanska, and T. Mark Fromhold. 2021.
512 "Universal Mobility Characteristics of Graphene Originating from Charge Scattering by Ionised
513 Impurities." *Communications Physics* 4 (1). <https://doi.org/10.1038/s42005-021-00518-2>.
- 514 Goutelle, Sylvain, Michel Maurin, Florent Rougier, Xavier Barbaut, Laurent Bourguignon, Michel Ducher,
515 and Pascal Maire. 2008. "The Hill Equation: A Review of Its Capabilities in Pharmacological
516 Modelling." *Fundamental and Clinical Pharmacology*. [https://doi.org/10.1111/j.1472-](https://doi.org/10.1111/j.1472-8206.2008.00633.x)
517 [8206.2008.00633.x](https://doi.org/10.1111/j.1472-8206.2008.00633.x).
- 518 Gray, Mason J., Narendra Kumar, Ryan O'Connor, Marcel Hoek, Erin Sheridan, Meaghan C. Doyle, Marisa
519 L. Romanelli, et al. 2020. "A Cleanroom in a Glovebox." *Review of Scientific Instruments* 91 (7):
520 073909. <https://doi.org/10.1063/5.0006462>.
- 521 Griffin, Justin H., and Kevin M. Downard. 2021. "Mass Spectrometry Analytical Responses to the SARS-
522 CoV2 Coronavirus in Review." *TrAC Trends in Analytical Chemistry* 142 (September): 116328.
523 <https://doi.org/10.1016/J.TRAC.2021.116328>.
- 524 Han, Mi Seon, Moon Woo Seong, Eun Young Heo, Ji Hong Park, Namhee Kim, Sue Shin, Sung Im Cho,
525 Sung Sup Park, and Eun Hwa Choi. 2020. "Sequential Analysis of Viral Load in a Neonate and Her
526 Mother Infected with Severe Acute Respiratory Syndrome Coronavirus 2." *Clinical Infectious
527 Diseases* 71 (16): 2236–39. <https://doi.org/10.1093/cid/ciaa447>.
- 528 Hart, Olga E., and Rolf U. Halden. 2020. "Computational Analysis of SARS-CoV-2/COVID-19 Surveillance
529 by Wastewater-Based Epidemiology Locally and Globally: Feasibility, Economy, Opportunities and
530 Challenges." *Science of the Total Environment* 730: 138875.
531 <https://doi.org/10.1016/j.scitotenv.2020.138875>.
- 532 Heijnen, Leo, and Gertjan Medema. 2011. "Surveillance of Influenza A and the Pandemic Influenza A
533 (H1N1) 2009 in Sewage and Surface Water in the Netherlands."
534 <https://doi.org/10.2166/wh.2011.019>.
- 535 Henze, Mogens; van Loosdrecht, Mark; Ekama, George; Brdjanovic, Damir. 2008. "Biological Wastewater
536 Treatment - Google Books." In .

- 537 <https://books.google.com/books?hl=en&lr=&id=41JButufnm8C&oi=fnd&pg=PA33&dq=wastewater>
538 [+composition&ots=nUB5m3DG0n&sig=dZrAgPzITdRkngMOX-](https://books.google.com/books?hl=en&lr=&id=41JButufnm8C&oi=fnd&pg=PA33&dq=wastewater+composition&ots=nUB5m3DG0n&sig=dZrAgPzITdRkngMOX-)
539 [N3DoRvfM#v=onepage&q=wastewater+composition&f=false](https://books.google.com/books?hl=en&lr=&id=41JButufnm8C&oi=fnd&pg=PA33&dq=wastewater+composition&ots=nUB5m3DG0n&sig=dZrAgPzITdRkngMOX-N3DoRvfM#v=onepage&q=wastewater+composition&f=false).
- 540 Hsu, Shu Yu, Mohamed Bayati, Chenhui Li, Hsin Yeh Hsieh, Anthony Belenchia, Jessica Klutts, Sally A.
541 Zemmer, et al. 2022. "Biomarkers Selection for Population Normalization in SARS-CoV-2
542 Wastewater-Based Epidemiology." *Water Research* 223 (September): 118985.
543 <https://doi.org/10.1016/J.WATRES.2022.118985>.
- 544 https, Pearl, Vikram Srinivasa Raghavan, Theodore Bungon, Paul Davey, Toby Whitley, Shakil A Awan,
545 and Sai Siva Gorthi. 2022. "Aptamer Functionalisation of Back-Gated Graphene Field Effect
546 Transistors for Pb 2+ Sensing," 14–18. <https://doi.org/10.3390/xxxxx>.
- 547 Huang, Man Hong, Yong Mei Li, and Guo Wei Gu. 2010. "Chemical Composition of Organic Matters in
548 Domestic Wastewater." *Desalination* 262 (1–3): 36–42.
549 <https://doi.org/10.1016/j.desal.2010.05.037>.
- 550 Huang, Po Jung Jimmy, and Juewen Liu. 2022. "Selection of Aptamers for Sensing Caffeine and
551 Discrimination of Its Three Single Demethylated Analogues." *Analytical Chemistry* 94 (7): 3142–49.
552 https://doi.org/10.1021/ACS.ANALCHEM.1C04349/ASSET/IMAGES/LARGE/AC1C04349_0006.JPEG.
- 553 Huerta-Fontela, Maria, Maria Teresa Galceran, and Francesc Ventura. 2007. "Ultraperformance Liquid
554 Chromatography Tandem Mass Spectrometry Analysis of Stimulatory Drugs of Abuse in
555 Wastewater and Surface Waters." *Analytical Chemistry* 79 (10): 3821–29.
556 <https://doi.org/10.1021/AC062370X/ASSET/IMAGES/LARGE/AC062370XF00003.JPEG>.
- 557 Hwang, Michael T., B. Landon Preston, Lee Joon, Choi Duyoung, H. Mo Alexander, Glinsky Gennadi, and
558 Lal Ratnesh. 2016. "Highly Specific SNP Detection Using 2D Graphene Electronics and DNA Strand
559 Displacement." *Proceedings of the National Academy of Sciences of the United States of America*
560 113 (26): 7088–93.
561 https://doi.org/10.1073/PNAS.1603753113/SUPPL_FILE/PNAS.1603753113.SAPP.PDF.
- 562 Jones, David L., Marcos Quintela Baluja, David W. Graham, Alexander Corbishley, James E. McDonald,
563 Shelagh K. Malham, Luke S. Hillary, et al. 2020. "Shedding of SARS-CoV-2 in Feces and Urine and Its
564 Potential Role in Person-to-Person Transmission and the Environment-Based Spread of COVID-19."
565 *The Science of the Total Environment* 749 (December): 141364.
566 <https://doi.org/10.1016/J.SCITOTENV.2020.141364>.
- 567 Jones, Susan, David T.A. Daley, Nicholas M. Luscombe, Helen M. Berman, and Janet M. Thornton. 2001.
568 "Protein–RNA Interactions: a Structural Analysis." *Nucleic Acids Research* 29 (4): 943.
569 <https://doi.org/10.1093/NAR/29.4.943>.
- 570 Karthikeyan, Smruthi, Joshua I Levy, Peter De Hoff, Greg Humphrey, Amanda Birmingham, Kristen
571 Jepsen, Sawyer Farmer, et al. 2022. "Wastewater Sequencing Reveals Early Cryptic SARS-CoV-2
572 Variant Transmission." *Nature* 609 (7925): 101–8. <https://doi.org/10.1038/s41586-022-05049-6>.
- 573 Karthikeyan, Smruthi, Andrew Nguyen, Daniel McDonald, Yijian Zong, Nancy Ronquillo, Junting Ren,
574 Jingjing Zou, et al. 2021. "Rapid, Large-Scale Wastewater Surveillance and Automated COVID-19
575 Cases on a University Campus." *American Society for Microbiology* 6 (4): e00793-21.
- 576 Kasprzyk-Hordern, Barbara, Natalie Sims, Kata Farkas, Kishore Jagadeesan, Kathryn Proctor, Matthew J.
577 Wade, and Davey L. Jones. 2023. "Wastewater-Based Epidemiology for Comprehensive Community

- 578 Health Diagnostics in a National Surveillance Study: Mining Biochemical Markers in Wastewater.”
579 *Journal of Hazardous Materials* 450 (January): 130989.
580 <https://doi.org/10.1016/j.jhazmat.2023.130989>.
- 581 Ke, Zunlong, Joaquin Oton, Kun Qu, Mirko Cortese, Vojtech Zila, Lesley McKeane, Takanori Nakane, et al.
582 2020. “Structures and Distributions of SARS-CoV-2 Spike Proteins on Intact Virions.” *Nature* 2020
583 588:7838 588 (7838): 498–502. <https://doi.org/10.1038/s41586-020-2665-2>.
- 584 Khan, Niazul I., and Edward Song. 2021. “Detection of an IL-6 Biomarker Using a GFET Platform
585 Developed with a Facile Organic Solvent-Free Aptamer Immobilization Approach.” *Sensors* 2021,
586 Vol. 21, Page 1335 21 (4): 1335. <https://doi.org/10.3390/S21041335>.
- 587 Kohlberger, Michael, and Gabriele Gadermaier. 2022. “SELEX: Critical Factors and Optimization
588 Strategies for Successful Aptamer Selection.” *Biotechnology and Applied Biochemistry* 69 (5): 1771.
589 <https://doi.org/10.1002/BAB.2244>.
- 590 Kumar, Narendra, Mason Gray, Juan C. Ortiz-Marquez, Andrew Weber, Cameron R Desmond, Avni
591 Argun, Tim Opijnen, and Kenneth S Burch. 2020. “Detection of a Multi-disease Biomarker in Saliva
592 with Graphene Field Effect Transistors.” *MEDICAL DEVICES & SENSORS*, October, e10121.
593 <https://doi.org/10.1002/mds3.10121>.
- 594 Kumar, Narendra, Muhit Rana, Michael Geiwitz, Niazul Islam Khan, Matthew Catalano, Juan C Ortiz-
595 Marquez, Hikari Kitadai, et al. 2022. “Rapid, Multianalyte Detection of Opioid Metabolites in
596 Wastewater.” *ACS Nano* 16 (3): 3704–14. <https://doi.org/10.1021/acsnano.1c07094>.
- 597 Kumar, Narendra, Wenjian Wang, Juan C. Ortiz-Marquez, Matthew Catalano, Mason Gray, Nadia Biglari,
598 Kitadai Hikari, et al. 2020. “Dielectrophoresis Assisted Rapid, Selective and Single Cell Detection of
599 Antibiotic Resistant Bacteria with G-FETs.” *Biosensors and Bioelectronics* 156 (February): 112123.
600 <https://doi.org/10.1016/j.bios.2020.112123>.
- 601 Kwong Hong Tsang, Deana, Tyler J. Lieberthal, Clare Watts, Iain E. Dunlop, Sami Ramadan, Armando E.
602 del Rio Hernandez, and Norbert Klein. 2019. “Chemically Functionalised Graphene FET Biosensor
603 for the Label-Free Sensing of Exosomes.” *Scientific Reports* 2019 9:1 9 (1): 1–10.
604 <https://doi.org/10.1038/s41598-019-50412-9>.
- 605 Lafond, Kathryn E., Rachael M. Porter, Melissa J. Whaley, Zhou Suizan, Zhang Ran, Mohammad Abdul
606 Aleem, Binay Thapa, et al. 2021. “Global Burden of Influenza-Associated Lower Respiratory Tract
607 Infections and Hospitalizations among Adults: A Systematic Review and Meta-Analysis.” *PLOS*
608 *Medicine* 18 (3): e1003550. <https://doi.org/10.1371/JOURNAL.PMED.1003550>.
- 609 Lara-Jacobo, Linda R., Golam Islam, Jean Paul Desaulniers, Andrea E. Kirkwood, and Denina B.D.
610 Simmons. 2022. “Detection of SARS-CoV-2 Proteins in Wastewater Samples by Mass
611 Spectrometry.” *Environmental Science and Technology* 56 (8): 5062–70.
612 https://doi.org/10.1021/ACS.EST.1C04705/ASSET/IMAGES/LARGE/ES1C04705_0005.JPEG.
- 613 Leung, Nancy H L. 2021. “Transmissibility and Transmission of Respiratory Viruses.”
614 <https://doi.org/10.1038/s41579-021-00535-6>.
- 615 Li, Wnkui; Zhang, Ji; Tse, Francis L.S. 2013. *Handbook of LC-MS Bioanalysis: Best Practices, Experimental*
616 *Protocols, and ...* - Google Books.
617 [https://books.google.com/books?hl=en&lr=&id=xz7AEAAAQBAJ&oi=fnd&pg=PR11&dq=lc-
618 ms+protocol&ots=jwlHekwcxh&sig=gS2EDkTDLMpJFwfYtcF65uTlv2A#v=onepage&q=lc-ms](https://books.google.com/books?hl=en&lr=&id=xz7AEAAAQBAJ&oi=fnd&pg=PR11&dq=lc-ms+protocol&ots=jwlHekwcxh&sig=gS2EDkTDLMpJFwfYtcF65uTlv2A#v=onepage&q=lc-ms)

- 619 protocol&f=false.
- 620 Li, Chenhui, Mohamed Bayati, Shu-Yu Hsu, Hsin-Yeh Hsieh, Wilfing Lindsi, Anthony Belenchia, Sally A.
621 Zemmer, et al. 2022a. "Population Normalization in SARS-CoV-2 Wastewater-Based Epidemiology:
622 Implications from Statewide Wastewater Monitoring in Missouri." *MedRxiv*, September,
623 2022.09.08.22279459. <https://doi.org/10.1101/2022.09.08.22279459>.
- 624 ——. 2022b. "Population Normalization in SARS-CoV-2 Wastewater-Based Epidemiology: Implications
625 from Statewide Wastewater Monitoring in Missouri." *MedRxiv*, September, 2022.09.08.22279459.
626 <https://doi.org/10.1101/2022.09.08.22279459>.
- 627 Li, Jiahao, Ding Wu, Yi Yu, Tingxian Li, Kun Li, Meng Meng Xiao, Yirong Li, Zhi Yong Zhang, and Guo Jun
628 Zhang. 2021. "Rapid and Unamplified Identification of COVID-19 with Morpholino-Modified
629 Graphene Field-Effect Transistor Nanosensor." *Biosensors and Bioelectronics* 183 (July): 113206.
630 <https://doi.org/10.1016/j.BIOS.2021.113206>.
- 631 Lorenzo, Maria, and Yolanda Picó. 2019. "Wastewater-Based Epidemiology: Current Status and Future
632 Prospects." *Current Opinion in Environmental Science and Health* 9: 77–84.
633 <https://doi.org/10.1016/j.coesh.2019.05.007>.
- 634 Lores, Emile M., and Jonathan R. Pennock. 1998. "The Effect of Salinity on Binding of Cd, Cr, Cu and Zn to
635 Dissolved Organic Matter." *Chemosphere* 37 (5): 861–74. [https://doi.org/10.1016/S0045-
636 6535\(98\)00090-3](https://doi.org/10.1016/S0045-6535(98)00090-3).
- 637 Lowry, Sarah A., Marlene K. Wolfe, and Alexandria B. Boehm. 2023. "Respiratory Virus Concentrations in
638 Human Excretions That Contribute to Wastewater: A Systematic Review and Meta-Analysis."
639 *Journal of Water and Health* 21 (6): 831–48. <https://doi.org/10.2166/WH.2023.057>.
- 640 Lu, Hsiang Wei, Alexander A. Kane, Jonathan Parkinson, Yingning Gao, Reza Hajian, Michael Heltzen,
641 Brett Goldsmith, and Kiana Aran. 2022. "The Promise of Graphene-Based Transistors for
642 Democratizing Multiomics Studies." *Biosensors and Bioelectronics* 195 (January): 113605.
643 <https://doi.org/10.1016/j.BIOS.2021.113605>.
- 644 Madhi, Shabir A., Fernando P. Polack, Pedro A. Piedra, Flor M. Munoz, Adrian A. Trenholme, Eric A.F.
645 Simões, Geeta K. Swamy, et al. 2020. "Respiratory Syncytial Virus Vaccination during Pregnancy
646 and Effects in Infants." *New England Journal of Medicine* 383 (5): 426–39.
647 https://doi.org/10.1056/NEJMOA1908380/SUPPL_FILE/NEJMOA1908380_DATA-SHARING.PDF.
- 648 Massano, Marta, Alberto Salomone, Enrico Gerace, Eugenio Alladio, Marco Vincenti, and Marco Minella.
649 2023. "Wastewater Surveillance of 105 Pharmaceutical Drugs and Metabolites by Means of Ultra-
650 High-Performance Liquid-Chromatography-Tandem High Resolution Mass Spectrometry." *Journal*
651 *of Chromatography. A* 1693: 463896. <https://doi.org/10.1016/j.chroma.2023.463896>.
- 652 Medema, Gertjan, Frederic Been, Leo Heijnen, and Susan Petterson. 2020. "Implementation of
653 Environmental Surveillance for SARS-CoV-2 Virus to Support Public Health Decisions: Opportunities
654 and Challenges." *Current Opinion in Environmental Science and Health* 17: 49–71.
655 <https://doi.org/10.1016/j.coesh.2020.09.006>.
- 656 Mestankova, Hana, Kristin Schirmer, Beate I. Escher, Urs Von Gunten, and Silvio Canonica. 2012.
657 "Removal of the Antiviral Agent Oseltamivir and Its Biological Activity by Oxidative Processes."
658 *Environmental Pollution* 161: 30–35. <https://doi.org/10.1016/j.envpol.2011.09.018>.
- 659 Metabolite, Molnupiravir, Timofey Komarov, Polina Karnakova, Olga Archakova, Dana Shchelgacheva,

- 660 Natalia Bagaeva, Mariia Popova, et al. 2023. "Chromatography with Tandem Mass Spectrometry
661 (HPLC-MS/MS) Method for Quantification of Major Development and Validation of a High-
662 Performance Liquid Chromatography with Tandem Mass Spectrometry (HPLC-MS/MS) Method for
663 Quantification of Major Molnupiravir Metabolite (β -D-N4-Hydroxycytidine) in Human Plasma."
664 <https://doi.org/10.3390/biomedicines11092356>.
- 665 Nekrasov, Nikita, Stefan Jaric, Dmitry Kireev, Aleksei V. Emelianov, Alexey V. Orlov, Ivana Gadjanski, Petr
666 I. Nikitin, Deji Akinwande, and Ivan Bobrinetskiy. 2022. "Real-Time Detection of Ochratoxin A in
667 Wine through Insight of Aptamer Conformation in Conjunction with Graphene Field-Effect
668 Transistor." *Biosensors and Bioelectronics* 200 (March): 113890.
669 <https://doi.org/10.1016/J.BIOS.2021.113890>.
- 670 Nemudryi, Artem, Anna Nemudraia, Tanner Wiegand, Kevin Surya, Murat Buyukyoruk, Calvin Cicha, Karl
671 K. Vanderwood, Royce Wilkinson, and Blake Wiedenheft. 2020. "Temporal Detection and
672 Phylogenetic Assessment of SARS-CoV-2 in Municipal Wastewater." *Cell Reports Medicine* 1 (6).
673 <https://doi.org/10.1016/J.XCRM.2020.100098>.
- 674 Nikolaev, Evgeny N., Maria I. Indeykina, Alexander G. Brzhozovskiy, Anna E. Bugrova, Alexey S.
675 Kononikhin, Natalia L. Starodubtseva, Evgeny V. Petrotchenko, Grigoriy I. Kovalev, Christoph H.
676 Borchers, and Gennady T. Sukhikh. 2020. "Mass-Spectrometric Detection of SARS-CoV-2 Virus in
677 Scrapings of the Epithelium of the Nasopharynx of Infected Patients via Nucleocapsid N Protein."
678 *Journal of Proteome Research* 19 (11): 4393–97.
679 https://doi.org/10.1021/ACS.JPROTEOME.0C00412/ASSET/IMAGES/MEDIUM/PROC00412_0003.GIF.
680 F.
- 681 Novo, Ana, Sandra André, Paula Viana, Olga C. Nunes, and Célia M. Manaia. 2013. "Antibiotic Resistance,
682 Antimicrobial Residues and Bacterial Community Composition in Urban Wastewater." *Water*
683 *Research* 47 (5): 1875–87. <https://doi.org/10.1016/j.watres.2013.01.010>.
- 684 Pan, Yang, Daitao Zhang, Peng Yang, Leo L.M. Poon, and Quanyi Wang. 2020. "Viral Load of SARS-CoV-2
685 in Clinical Samples." *The Lancet. Infectious Diseases* 20 (4): 411. [https://doi.org/10.1016/S1473-3099\(20\)30113-4](https://doi.org/10.1016/S1473-3099(20)30113-4).
- 687 Pawar, Pratik. 2023. "Tracking RSV in Low- and Middle-Income Countries." *Nature* 621 (7980): S62–63.
688 <https://doi.org/10.1038/D41586-023-02960-4>.
- 689 Peccia, Jordan, Alessandro Zulli, Doug E. Brackney, Nathan D. Grubaugh, Edward H. Kaplan, Arnau
690 Casanovas-Massana, Albert I. Ko, et al. 2020. "Measurement of SARS-CoV-2 RNA in Wastewater
691 Tracks Community Infection Dynamics." *Nature Biotechnology* 38 (10): 1164.
692 <https://doi.org/10.1038/S41587-020-0684-Z>.
- 693 Peng, Jiaxi, Jianxian Sun, Mingqing Ivy Yang, Richard M. Gibson, Eric J. Arts, Abayomi S. Olabode, Art F.Y.
694 Poon, et al. 2022. "Early Warning Measurement of SARS-CoV-2 Variants of Concern in Wastewaters
695 by Mass Spectrometry." *Environmental Science and Technology Letters* 9 (7): 638–44.
696 https://doi.org/10.1021/ACS.ESTLETT.2C00280/ASSET/IMAGES/LARGE/EZ2C00280_0003.JPEG.
- 697 Percze, Krisztina, Zoltán Szakács, Éva Scholz, Judit András, Zsuzsanna Szeitner, Corné H Van Den
698 Kieboom, Gerben Ferwerda, Marien I De Jonge, Róbert E Gyurcsányi, and Tamás Mészáros. 2017.
699 "Aptamers for Respiratory Syncytial Virus Detection OPEN." <https://doi.org/10.1038/srep42794>.
- 700 Picó, Yolanda, and Damià Barceló. 2021. "Mass Spectrometry in Wastewater-Based Epidemiology for the
701 Determination of Small and Large Molecules as Biomarkers of Exposure: Toward a Global View of

- 702 Environment and Human Health under the COVID-19 Outbreak.” *ACS Omega* 6 (46): 30865–72.
703 https://doi.org/10.1021/ACSOMEGA.1C04362/ASSET/IMAGES/LARGE/AO1C04362_0002.JPEG.
- 704 Ping, Jinglei, Ramya Vishnubhotla, Amey Vrudhula, and A. T. Charlie Johnson. 2016a. “Scalable
705 Production of High-Sensitivity, Label-Free DNA Biosensors Based on Back-Gated Graphene Field
706 Effect Transistors.” *ACS Nano* 10 (9): 8700–8704.
707 https://doi.org/10.1021/ACSNANO.6B04110/ASSET/IMAGES/LARGE/NN-2016-04110P_0005.JPEG.
- 708 Ping, Jinglei, Ramya Vishnubhotla, Amey Vrudhula, and A T Charlie Johnson. 2016b. “Scalable Production
709 of High-Sensitivity, Label-Free DNA Biosensors Based on Back-Gated Graphene Field Effect
710 Transistors.” *Acs Nano* 10 (9): 8700–8704. <https://doi.org/10.1021/acsnano.6b04110>.
- 711 Pinto, Artur M., Inês C. Gonçalves, and Fernão D. Magalhães. 2013. “Graphene-Based Materials
712 Biocompatibility: A Review.” *Colloids and Surfaces B: Biointerfaces* 111 (November): 188–202.
713 <https://doi.org/10.1016/J.COLSURFB.2013.05.022>.
- 714 Qian, Shuwen, Dingran Chang, Sisi He, and Yingfu Li. 2022. “Aptamers from Random Sequence Space:
715 Accomplishments, Gaps and Future Considerations.” *Analytica Chimica Acta* 1196 (March): 339511.
716 <https://doi.org/10.1016/J.ACA.2022.339511>.
- 717 Rainey, Andrew L., Song Liang, Joseph H. Bisesi, Tara Sabo-Attwood, and Anthony T. Maurelli. 2023. “A
718 Multistate Assessment of Population Normalization Factors for Wastewater-Based Epidemiology of
719 COVID-19.” *PLOS ONE* 18 (4): e0284370. <https://doi.org/10.1371/JOURNAL.PONE.0284370>.
- 720 Rames, Emily K., and Joanne Macdonald. 2019. “Rapid Assessment of Viral Water Quality Using a Novel
721 Recombinase Polymerase Amplification Test for Human Adenovirus.” *Applied Microbiology and
722 Biotechnology* 103 (19): 8115–25. <https://doi.org/10.1007/S00253-019-10077-W/TABLES/2>.
- 723 Rodrigues, Teresa, Vladyslav Mishyn, Yann R. Leroux, Laura Butruille, Eloise Woitrain, Alexandre Barras,
724 Patrik Aspermaier, et al. 2022. “Highly Performing Graphene-Based Field Effect Transistor for the
725 Differentiation between Mild-Moderate-Severe Myocardial Injury.” *Nano Today* 43: 101391.
726 <https://doi.org/10.1016/j.nantod.2022.101391>.
- 727 Rouzé, Anahita, Ignacio Martin-Loeches, Pedro Pova, Demosthenes Makris, Antonio Artigas, Mathilde
728 Bouchereau, Fabien Lambiotte, et al. 2021. “Relationship between SARS-CoV-2 Infection and the
729 Incidence of Ventilator-Associated Lower Respiratory Tract Infections: A European Multicenter
730 Cohort Study.” *Intensive Care Med* 47: 188–98. <https://doi.org/10.1007/s00134-020-06323-9>.
- 731 Sender, Ron, Yinon M. Bar-On, Shmuel Gleizer, Biana Bernsthein, Avi Flamholz, Rob Phillips, and Ron
732 Milo. 2020. “The Total Number and Mass of SARS-CoV-2 Virions.” *MedRxiv*, November.
733 <https://doi.org/10.1101/2020.11.16.20232009>.
- 734 Seo, Giwan, Geonhee Lee, Mi Jeong Kim, Seung Hwa Baek, Minsuk Choi, Keun Bon Ku, Chang Seop Lee,
735 et al. 2020a. “Rapid Detection of COVID-19 Causative Virus (SARS-CoV-2) in Human
736 Nasopharyngeal Swab Specimens Using Field-Effect Transistor-Based Biosensor.” *ACS Nano* 14 (4):
737 5135–42.
738 https://doi.org/10.1021/ACSNANO.0C02823/ASSET/IMAGES/LARGE/NN0C02823_0006.JPEG.
- 739 ——. 2020b. “Rapid Detection of COVID-19 Causative Virus (SARS-CoV-2) in Human Nasopharyngeal
740 Swab Specimens Using Field-Effect Transistor-Based Biosensor.” *ACS Nano* 14 (4): 5135–42.
741 https://doi.org/10.1021/ACSNANO.0C02823/ASSET/IMAGES/LARGE/NN0C02823_0006.JPEG.
- 742 Shiratori, Ikuo, Joe Akitomi, David A. Boltz, Katsunori Horii, Makio Furuichi, and Iwao Waga. 2014.

- 743 “Selection of DNA Aptamers That Bind to Influenza A Viruses with High Affinity and Broad Subtype
744 Specificity.” *Biochemical and Biophysical Research Communications* 443 (1): 37–41.
745 <https://doi.org/10.1016/j.bbrc.2013.11.041>.
- 746 Stern, Eric. 2007. “Label-Free Sensing with Semiconducting Nanowires.”
- 747 Street, Renée, Shirley Malema, Nomfundo Mahlangeni, and Angela Mathee. 2020. “Wastewater
748 Surveillance for Covid-19: An African Perspective.” *Science of the Total Environment* 743: 2018–20.
749 <https://doi.org/10.1016/j.scitotenv.2020.140719>.
- 750 Sweetapple, Chris, Matthew J. Wade, Peter Melville-Shreeve, Albert S. Chen, Chris Lilley, Jessica Irving,
751 Jasmine M.S. Grimsley, and Joshua T. Bunce. 2023. “Dynamic Population Normalisation in
752 Wastewater-Based Epidemiology for Improved Understanding of the SARS-CoV-2 Prevalence: A
753 Multi-Site Study.” *Journal of Water and Health* 21 (5): 625–42.
754 <https://doi.org/10.2166/WH.2023.318>.
- 755 Szunerits, Sabine, Teresa Rodrigues, Rupali Bagale, Henri Happy, Rabah Boukherroub, and Wolfgang
756 Knoll. 2023. “Graphene-Based Field-Effect Transistors for Biosensing: Where Is the Field Heading
757 To?” *Analytical and Bioanalytical Chemistry*, June, 1–14. [https://doi.org/10.1007/S00216-023-](https://doi.org/10.1007/S00216-023-04760-1/TABLES/1)
758 [04760-1/TABLES/1](https://doi.org/10.1007/S00216-023-04760-1/TABLES/1).
- 759 Urmann, Katharina, Julia Modrejewski, Thomas Scheper, and Johanna G. Walter. 2017. “Aptamer-
760 Modified Nanomaterials: Principles and Applications.” *BioNanoMaterials* 18 (1–2): 20160012.
761 https://doi.org/10.1515/BNM-2016-0012/ASSET/GRAPHIC/J_BNM-2016-0012_FIG_001.JPG.
- 762 Velusamy, Karthik, Selvakumar Periyasamy, P Senthil Kumar, Gayathri Rangasamy, J Mercy, Nisha
763 Pauline, Pradeep Ramaraju, Sneka Mohanasundaram, and Dai-Viet Nguyen Vo. 2022. “Biosensor
764 for Heavy Metal Detection in Wastewater: A Review.” *Food and Chemical Toxicology* 168: 278–
765 6915. <https://doi.org/10.1016/j.fct.2022.113307>.
- 766 Wang, Chih-Hung, Chih-Peng Chang, and Gwo-Bin Lee. 2016. “Integrated Microfluidic Device Using a
767 Single Universal Aptamer to Detect Multiple Types of Influenza Viruses \$.”
768 <https://doi.org/10.1016/j.bios.2016.06.071>.
- 769 Wang, Hao, Zhuang Hao, Cong Huang, Feiran Li, and Yunlu Pan. 2023. “Monitoring Cd²⁺ in Oily
770 Wastewater Using an Aptamer-Graphene Field-Effect Transistor with a Selective Wetting Surface
771 †.” <https://doi.org/10.1039/d2na00416j>.
- 772 Wölfel, Roman, Victor M. Corman, Wolfgang Guggemos, Michael Seilmaier, Sabine Zange, Marcel A.
773 Müller, Daniela Niemeyer, et al. 2020. “Virological Assessment of Hospitalized Patients with COVID-
774 2019.” *Nature* 2020 581:7809 581 (7809): 465–69. <https://doi.org/10.1038/s41586-020-2196-x>.
- 775 World Health Organization. 2014. “The Top 10 Causes of Death.” 2014. [https://www.who.int/news-](https://www.who.int/news-room/fact-sheets/detail/the-top-10-causes-of-death)
776 [room/fact-sheets/detail/the-top-10-causes-of-death](https://www.who.int/news-room/fact-sheets/detail/the-top-10-causes-of-death).
- 777 Wu, Guangfu, Xin Tang, M Meyyappan, and King Wai Chiu Lai. 2017. “Doping Effects of Surface
778 Functionalization on Graphene with Aromatic Molecule and Organic Solvents.” *Applied Surface*
779 *Science* 425: 713–21. <https://doi.org/10.1016/j.apsusc.2017.07.048>.
- 780 Wu, Yuangen, Shenshan Zhan, Lumei Wang, and Pei Zhou. 2014. “Selection of a DNA Aptamer for
781 Cadmium Detection Based on Cationic Polymer Mediated Aggregation of Gold Nanoparticles.”
782 *Analyst* 139 (6): 1550–61. <https://doi.org/10.1039/C3AN02117C>.

- 783 Zang, Ruochen, Maria Florencia Gomez Castro, Broc T. McCune, Qiru Zeng, Paul W. Rothlauf, Naomi M.
784 Sonnek, Zhuoming Liu, et al. 2020. "TMPRSS2 and TMPRSS4 Promote SARS-CoV-2 Infection of
785 Human Small Intestinal Enterocytes." *Science Immunology* 5 (47).
786 <https://doi.org/10.1126/SCIIMMUNOL.ABC3582>.
- 787 Zhang, Ning, Yuhuan Gong, Fanping Meng, Yuhai Bi, Penghui Yang, and Fusheng Wang. 2020. "Virus
788 Shedding Patterns in Nasopharyngeal and Fecal Specimens of COVID-19 Patients." *MedRxiv*, March,
789 2020.03.28.20043059. <https://doi.org/10.1101/2020.03.28.20043059>.
- 790 Zhang, Yang, Mario Juhas, and Chun Kit Kwok. 2022. "Aptamers Targeting SARS-COV-2: A Promising Tool
791 to Fight against COVID-19." <https://doi.org/10.1016/j.tibtech.2022.07.012>.
- 792 Zhang, Zijie, Richa Pandey, Jiuxing Li, Jimmy Gu, Dawn White, Hannah D. Stacey, Jann C. Ang, et al. 2021.
793 "High-Affinity Dimeric Aptamers Enable the Rapid Electrochemical Detection of Wild-Type and
794 B.1.1.7 SARS-CoV-2 in Unprocessed Saliva." *Angewandte Chemie - International Edition* 60 (45):
795 24266–74. <https://doi.org/10.1002/ANIE.202110819>.
- 796 Zhou, Jiehua, and John Rossi. 2017. "Aptamers as Targeted Therapeutics: Current Potential and
797 Challenges." *Nature Reviews. Drug Discovery* 16 (3): 181. <https://doi.org/10.1038/NRD.2016.199>.
- 798

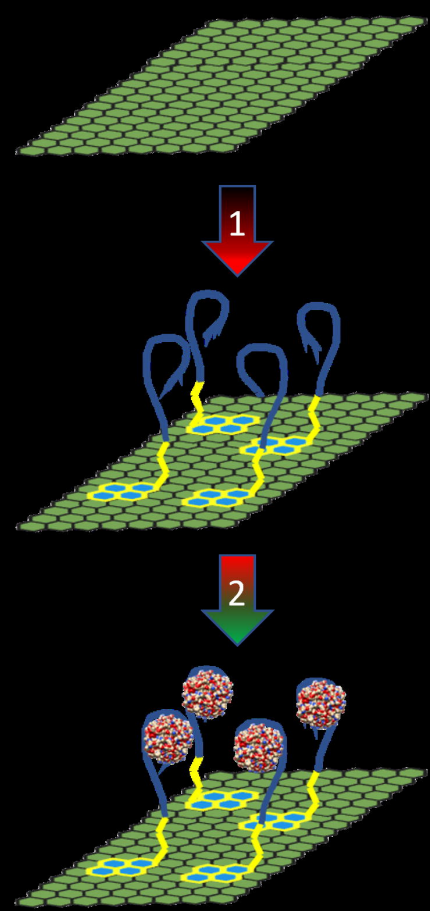
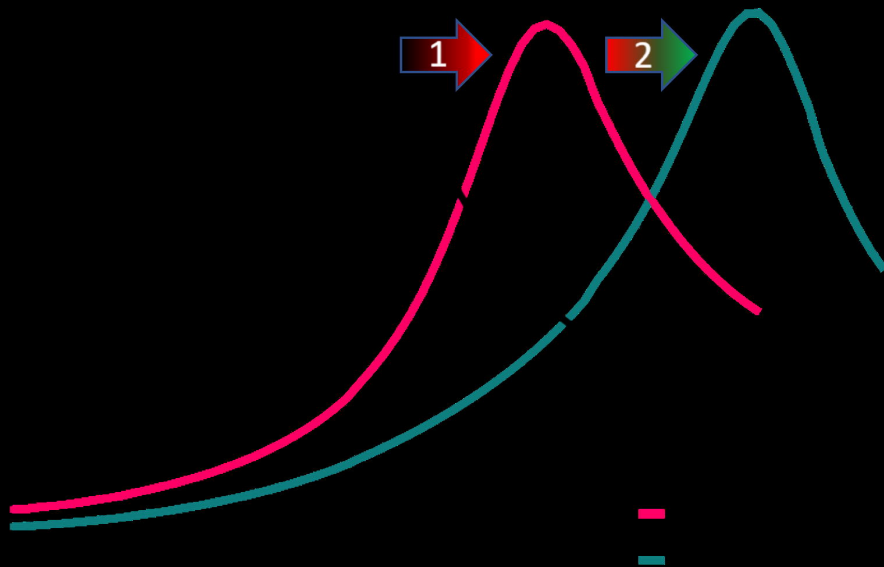
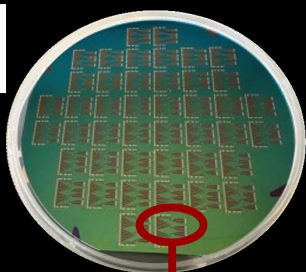


Fig. 1 – Dirac voltage shifting with aptamer and target attachment: The plot on the left shows the positive shift in the Dirac point (peak of the curves) from the intrinsic position of the bare graphene (black) of approximately 0.6V. After a 2:1 mixture of the aptamer probe to PEG is added the Dirac point shifts positively to about 0.8V (pink). A large shift in the Dirac point to 1.2V is then seen (green) in the presence of 1ng/ml of the target protein for SARS-CoV-2. On the right is a schematic of the bare graphene, aptamer attachment, and target attachment.

(a)



(b)

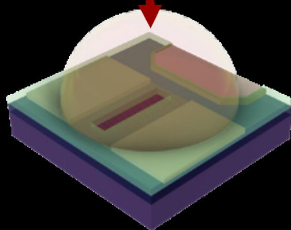
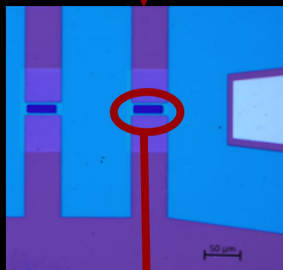
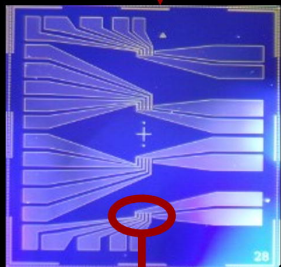
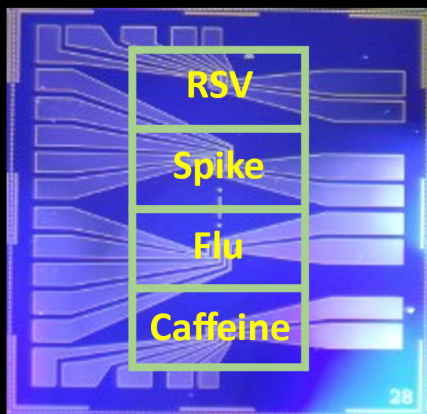


Fig. 2 – (a) Top: Wafer as fully fabricated. Second from top: Overview of the 1.2cm x 1.2cm GFET sensing platform. Third from top: 20x microscope image of a single sensing well. Two graphene devices and the coplanar gate electrode are shown. Bottom: Diagram of a single, functionalized graphene device during the sensing process. (b) Schematic of individual chip with PDMS well and labeled with functionalization for specific analytes.

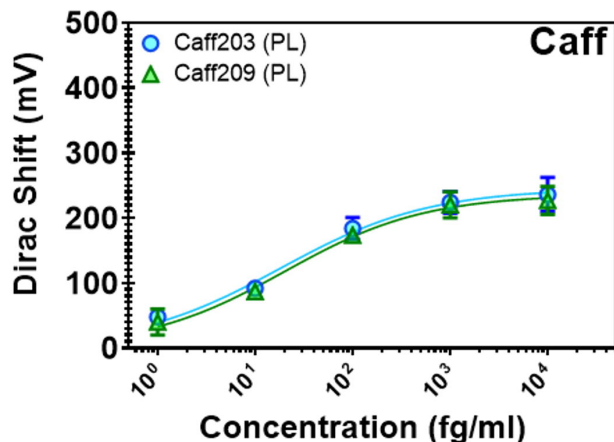
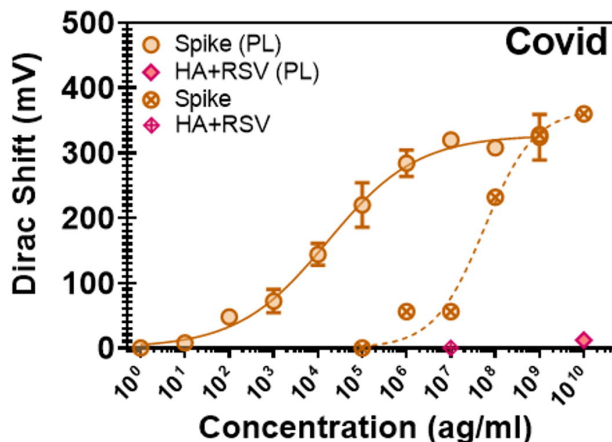
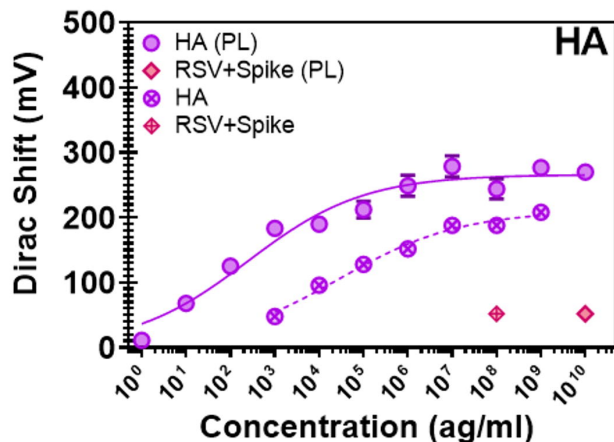
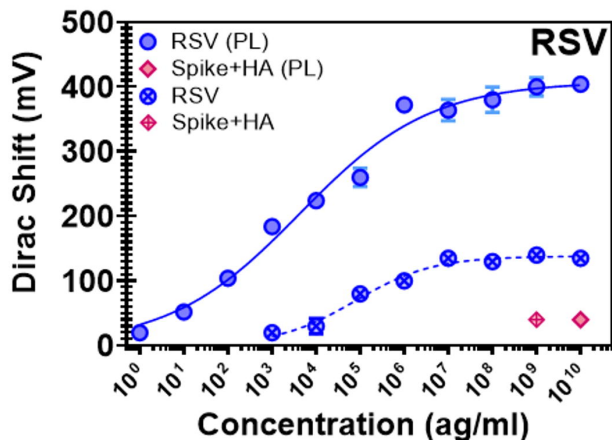


Fig. 3 –Concentration dependance measurements of viral proteins in PBS. Error bars calculated from the five GFETs per sensing well. Data points with crosses and dashed curves indicate non-pre-linked aptamers were used. Top Left - Influenza A Hemagglutinin detection. High concentrations of RSV and COVID Spike proteins used as a negative control. (PL) denotes pre-linked aptamer experiment. Top Right and Bottom Left - Same as in HA plot but with SARS-CoV-2 Spike and RSV proteins, respectively. Non-target proteins used as negative control in each case. Bottom Right - Concentration dependence measurements of two caffeine aptamers. Caffeine measurements were only conducted with pre-linked aptamers.

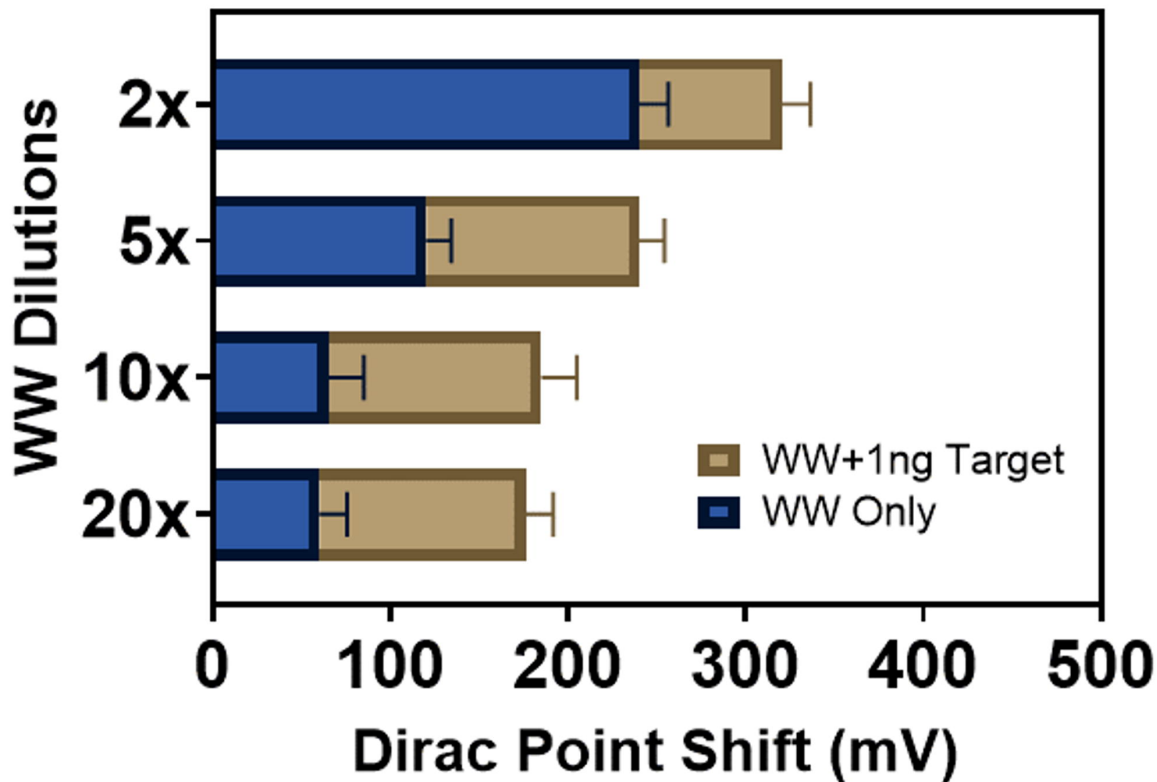


Fig. 4 – Histogram of the average Dirac point shift at various wastewater dilutions. The blue areas show the average Dirac point shift for five GFET devices after incubation of diluted wastewater for one hour. The tan areas show the further Dirac point shift after incubating the GFETs for one hour with 1ng/ml of target protein in their respective wastewater dilutions.

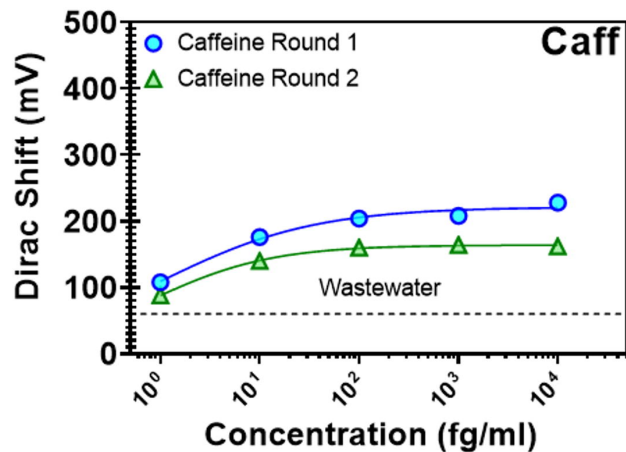
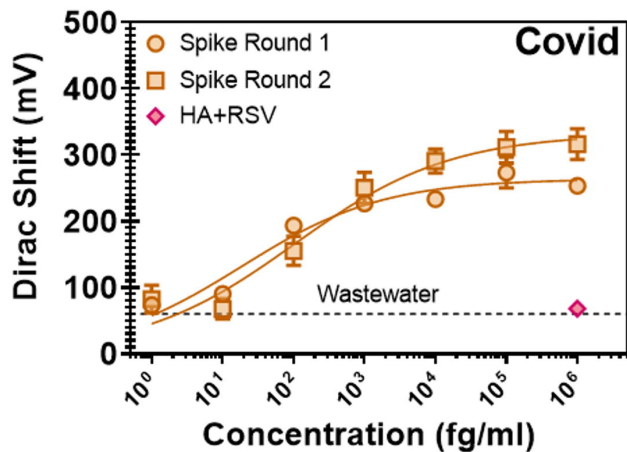
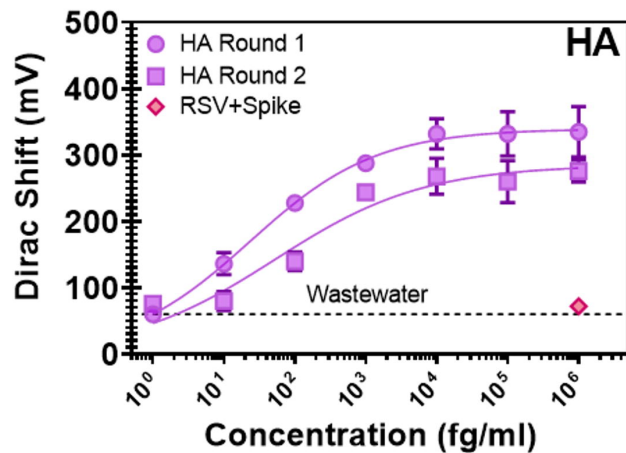
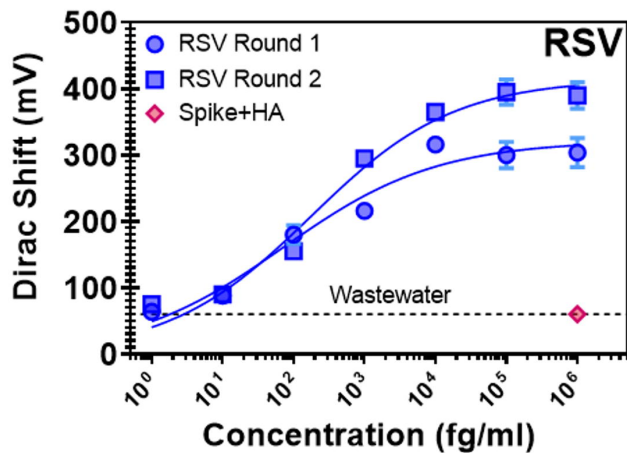


Fig. 5 – Concentration dependence measurements of viral proteins and caffeine in wastewater. Error bars calculated from the five GFETs per sensing well. From left to right, HA, RSV, and COVID spike proteins and Caffeine. Horizontal dashed line shows intrinsic background shift from the wastewater itself.

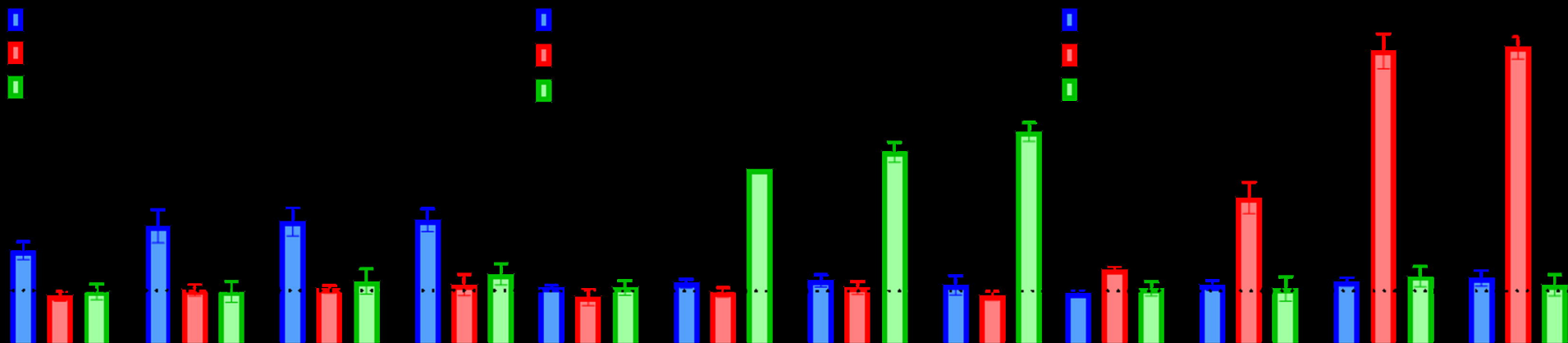


Fig. 6 – Wastewater Blind Tests: Each plot represents the differing concentrations for a coded sample. The assorted colors indicate the aptamer used in each well; blue for the 1C (Covid), red for H8 (RSV), and green for UA (Flu). The horizontal dotted line is the intrinsic shift from the wastewater. M.G. found that 1738 was COVID spike proteins (left), 1993 was HA (middle), and 2930 was RSV. Each was confirmed by O.R.P.'s written records.